ELSEVIER

Biophysical Chemistry 125 (2007) 72–91

Biophysical Chemistry

http://www.elsevier.com/locate/biophyschem

Effects of metal ion and solute conformation change on hydration of small amino acid

Natthiya Deeying, Kritsana Sagarik *

School of Chemistry, Institute of Science, Suranaree University of Technology, Nakhon Ratchasima 30000, Thailand

Received 13 April 2006; received in revised form 27 June 2006; accepted 27 June 2006
Available online 4 August 2006

Abstract

The effects of metal ion and solute conformation change on the structures, energetic and dynamics of water molecules in the first hydration shell of amino acid were studied, using three forms of alanine (Ala) and Li^+/Ala as model molecules. The theoretical investigations were started with construction of the test-particle model (T-model) potentials for all molecules involved and followed by molecular dynamics (MD) simulations of $[Ala]_{aq}$ and $[Li^+/Ala]_{aq}$ at 298 K. The MD results showed that the hydrogen bond (H-bond) networks of water at the functional groups of Ala are strengthened by the metal ion binding, whereas the rotation of the N–C^{α} bond from the angle $\phi = 0°$ to 180° brings about smaller effects which cannot be generalized. It was also shown that the dynamics of water molecule in the first hydration shell of amino acid could be estimated from the total–average potential energy landscapes and the water exchange diagrams. The MD results suggested inclusion of an additional dynamic step in the water exchange process, in which water molecule moves inside a channel within the first hydration shell of solute, before leaving the channel at some point. The theoretical results reported in the present work iterated the necessity to include explicit water molecules in the model calculations.

Keywords: Alanine; Lithium ion; Hydration; T-model; Residence time; Molecular dynamics simulations; Conformation

1. Introduction

It has been well established that metal ions play central roles in various processes in biological systems [1,2]. They are generally involved in enzyme regulation, stabilization of structures of reactive biomolecules [1,3], transportation to transmembrane channels, etc. [4]. Attempts have been made in the past decades to study structural and energetic aspects of metal ion-protein complexes in aqueous solutions and crystals [1]. These represent difficult tasks due to the fact that proteins are complicated multifunctional macromolecules with several possible conformations and binding sites. Based on theoretical and experimental studies, it appeared for example that, the positions of metal ion binding sites play critical roles in determining the locations of bond formations and disruptions in biochemical reactions [5]. In aqueous solutions, the stability of proteins and the folding patterns of the peptide backbones have been pointed out to be affected by the presence of metal ion [6]. Since there have been many review articles taking into account the interactions in protein solutions in details [7], only some important theoretical and experimental aspects relevant to the present study will be briefly summarized.

The affinities of metal ions with small amino acids, such as glycine (Gly) and alanine (Ala), as well as the dipeptides composed of these small amino acids such as Gly–Gly and Ala–Ala, in the gas phase have been investigated, using both experiments [8–11] and *ab initio* calculations [9,12–14]. The theoretical results obtained from the hybrid B3LYP exchange-correlation functional using extended basis sets revealed that, for Gly and Ala, the metal ion affinities decrease on going from Cu^+ to Li^+ and Na^+ and the values computed at this level of theory agree in general with experiments [13]; except for Li^+, for which a deviation of about 29 kJ/mol was observed. It appeared that, in the gas phase, the metal ions considered in Refs. [13,15] prefer to bind simultaneously at the N and O atoms of Gly and Ala. This type of bidentate coordination has been found also in larger amino acid complexes, such as Li^+/valine (Li^+/Val) [10], Na^+/phenylalanine (Na^+/Phe) [16], etc.

The influence of metal ions on the stability of small hydrogen bond (H-bond) complexes [17,18], as well as biologically active molecules, such as the base pairs of DNA [19,20], was reported

* Corresponding author. Tel./fax: +66 44 224635.
E-mail address: kritsana@sut.ac.th (K. Sagarik).

0301-4622/$ - see front matter © 2006 Elsevier B.V. All rights reserved.
doi:10.1016/j.bpc.2006.06.016

based on theoretical studies. *Ab initio* calculations in Ref. [18] showed that Li^+ transfers its electrostatic effects along the O=C–N structure in the formamide (FA)–H_2O complex, leading to a net stabilization effect (NSE) at the neighboring N–H…Ow H-bond. This was supported by the results obtained from FTIR experiment [21], which shows that, due to the condensing effects, Ag^+ and Zn^{2+} could give rise to an increase in the intermolecular H-bond interactions between adjacent molecules in the *N*-octadecanoyl-L-alanine monolayes; whereas the expanding effects of Ca^{2+}, Cd^{2+}, Ni^{2+} and La^{3+} could lead to the formation of intramolecular H-bonds.

Structures, energetic and dynamics of water molecules in the hydration shells of proteins have been pointed out to constitute basic information required to characterize their stability in aqueous solutions [22]. They have long been the subject of interest in both theoretical and experimental points of view [23–26], e.g. *ab initio* calculations, molecular dynamics (MD) and Monte Carlo (MC) simulations [27,28], as well as X-ray [29] and NMR experiments [30,31]. In aqueous solutions and crystals, X-ray crystallography measures the extent to which specific hydration sites of proteins are occupied by water molecules, whereas the observations of the Nuclear Overhauser Effects (NOE) between individual protons of amino acid residues and those of sufficiently tightly bound water enable NMR experiments to monitor specific water molecules in the hydration shells of proteins, before being replaced by another water molecule [32]. Through the measurements of NOE, the dynamics of individual water molecules in the hydration shells of proteins could be determined with acceptable accuracy [30,31], e.g. by measuring the residence times of specific water molecules. Although the residence times are sensitive to the definitions and methods employed in the investigations [33], the ones obtained from NMR experiments are compared well with those from MD simulations [30,31,34]. The residence times deduced from NMR experiments [35] suggested, for example, that the diffusion process of water molecules moving away from protein surface is heterogeneous; about 75% of the surface water diffuse 4 times slower and 25% diffuse 15 times faster than in the bulk. It was also illustrated based on MD simulations that the average residence times of water at the side chain atoms of proteins are approximately 50% smaller than for the backbone atoms [34,36].

Theoretical methods employed in the studies of solutions fall into two categories [37]; microscopic methods consider solvent molecules and their interactions with solutes explicitly, whereas macroscopic ones take into account solvent as a continuum medium characterized by a dielectric constant. It has been shown that both approaches have advantages and disadvantages. In our previous investigations [38–41], the H-bond networks of water in the first hydration shells of solutes were investigated using an explicit water model and MD simulations. The MD results showed that the H-bond networks in the first hydration shells of the zwitterionic form of Ala could be changed due to its conformation change [38], whereas the stability of the close-contact and solvent-separated guanidinium–formate (Gdm^+–FmO^-) complexes could be affected by the structures of the H-bond networks. These pieces of information suggested the necessity to include explicit water molecules in the model calculation [39].

In the present work, the effects of metal ion and solute conformation change on the structures, energetic and dynamics of water molecules in the first hydration shells of Ala were studied using MD simulations. The theoretical investigations were started with construction of the intermolecular potentials for the Ala–H_2O and Li^+/Ala–H_2O complexes using the test-particle model (T-model). They were applied in the calculations of equilibrium geometries and interaction energies of the Ala–H_2O and Li^+/Ala–H_2O complexes in the gas phase. *Ab initio* calculations at MP2 level were performed to check some of the T-model results. The T-model potentials were then applied in MD simulations of $[Ala]_{aq}$ and $[Li^+/Ala]_{aq}$ at 298 K, from which the three-dimensional structures and energetic of the H-bond networks of water in the first hydration shells were analyzed and visualized [42]. The dynamics of water molecules in the H-bond networks, such as the water exchange processes and the water residence times, were systematically studied and discussed based on the total–average potential energy landscapes and probability distribution (PD) maps [38,39,42]. The water exchange events in the first hydration shells in $[Ala]_{aq}$ and $[Li^+/Ala]_{aq}$ were further examined in details using water exchange diagrams [43,44], from which the water exchange pathways were identified and classified. The theoretical results obtained in the present investigations were discussed in comparison with available theoretical and experimental data of the same and similar systems.

2. Computational methods

In the gas phase, various experimental and theoretical evidences have led to the conclusion that both Gly and Ala exist in neutral forms [45,46], whereas in aqueous solutions and crystals, they adopt zwitterionic forms, abbreviated in the present study as Glyz and Alaz, respectively. Matrix isolation IR spectroscopy [47,48], microwave spectroscopy [49] and *ab initio* calculations [47,50–52] predicted at least three most stable conformations of Gly and Ala in the gas phase. They possess cyclic N–H…O=C, N…H–O and N–H…O–H intramolecular H-bonds, generally regarded as structures I, II and III, respectively. Structure I has been confirmed by *ab initio* calculations [47,50,52,53] and experiments [47,48] to represent the global minimum energy geometry, whereas structures II and III were reported to be local minimum energy geometries, with comparable relative stability [52,53]. *Ab initio* calculations at MP/6–31G(d) level predicted quite low interconversion energy barrier between structures III and I, only about 5.4 kJ/mol [53]. The situation is different in aqueous solutions, in which structure II [54] becomes the global minimum energy geometry and the proton transfer was suggested to take place readily between the O–H and N–H groups, forming Glyz and Alaz [47,51]. Although Glyz and Alaz dominate in aqueous solutions and crystals, their neutral forms could serve as model molecules in the studies of the hydration of the main chains, as well as the side chains, of proteins [54], which contain the N–H and C=O groups in general [55].

Since our main objectives were to study the effects of solute conformation change and metal ion on the hydration of model

amino acid in its neutral forms, three possible structures of Ala were considered. They are denoted by Ala-A, Ala-B and Ala-C in Fig. 1. Ala-A and Ala-B were chosen to illustrate the effects of conformation change, whereas Ala-C for the effects of metal ion. Ala-A represents the lowest minimum energy geometry of Ala in the gas phase, similar to structure I in Ref. [50]. The geometry of Ala-A was taken from Ref. [56] and reoptimized using *ab initio* calculations at MP2/6–311G(d,p) level, shown in our previous studies to be appropriate for the geometry optimizations of moderately strong H-bond systems, such as hydroxylamine [57] and benzoic acid (BA)–H_2O clusters [40]. Structure of Ala-B is slightly different from Ala-A, with the angle ϕ being 30° with respect to Ala-A. The structure of Ala-C is the same as structure IVp in Ref. [58], in which both N and O atoms are ready to form a bidentate coordination with metal ion [10,16]. Since the electrostatic effects were expected to dominate in Li^+/Ala-C, the basis set used in the geometry optimization was augmented with polarization and diffuse functions. The optimized geometries of Ala-A, Ala-B and Ala-C, as well as Li^+/Ala-C, were kept constants throughout the calculations.

2.1. The T-model potentials

In the T-model [38–41,57], the interaction energy ($\Delta E_{\text{T-model}}$) between molecules A and B is written as a sum of the first-order interaction energy (ΔE^1_{SCF}) and a higher-order term (ΔE^{r}).

$$\Delta E_{\text{T-model}} = \Delta E^1_{\text{SCF}} + \Delta E^{\text{r}} \tag{1}$$

ΔE^1_{SCF} in Eq. (1) accounts for the exchange repulsion and electrostatic energies which can be computed from *ab initio* first-order SCF calculations. ΔE^1_{SCF} takes the following analytical form:

$$\Delta E^1_{\text{SCF}} = \sum_{i\in\text{A}}\sum_{j\in\text{B}}\left[\exp\left(\frac{-R_{ij}+\sigma_i+\sigma_j}{\rho_i+\rho_j}\right)+\frac{q_iq_j}{R_{ij}}\right] \tag{2}$$

i and j in Eq. (2) label the sites of molecules A and B, respectively. σ_i, ρ_i and q_i are the site parameters; R_{ij} are the site–site distances. The exponential term in Eq. (2) is responsible for the size and shape of molecules A and B, with the site parameters σ_i and ρ_i, determined by probing molecules A and B with a test particle.

Since the structures and energetic of H-bond are determined to a large extent by the electrostatic energy, care must be exercised in the calculations of atomic charges, q_i and q_j in Eq. (2). Within the framework of the T-model, atomic charges are determined from the requirement that a point charge model reproduces the electrostatic potentials of molecules A and B. Our experience has shown that the charges obtained from the electrostatic potentials at the points selected according to the CHelpG scheme [59] work quite well with most H-bond systems considered [38–41,57]. In the present investigation, we, therefore, adopted the CHelpG scheme implemented in the Gaussian 98 package [60]. The electrostatic potentials employed in the calculations of the atomic charges were derived from *ab initio* calculations at MP2/6–311++G(d,p) level, which has been applied successfully in the calculations of the electron densities and atomic charges in conformers of Gly [58,61], using various theoretical models including the CHelpG scheme. For the molecules and complex considered here, more than nine

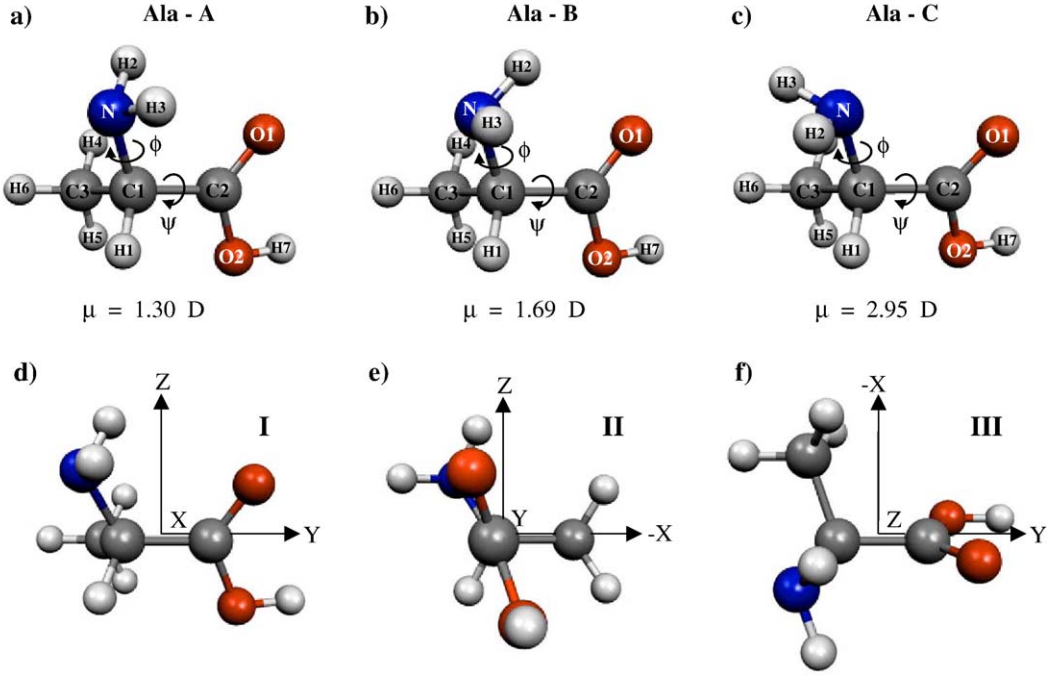

Fig. 1. Structures and atom numbering systems of Ala-A, Ala-B and Ala-C, together with the reference planes employed in MD analyses. Reference planes I, II and III are on the *YZ*, *XZ* and *XY* planes, respectively. The dipole moments (μ) were computed from the point charges derived from the CHelpG scheme [59].

thousand electrostatic energies were generated and employed in the calculations of the atomic charges. The dipole moments obtained from the CHelpG charges are also included in Fig. 1.

The higher-order term (ΔE^{r}) in Eq. (1) takes into account the dispersion and polarization contributions of the T-model potentials. ΔE^{r} could be determined from both theoretical and experimental data and takes the following analytical form:

$$\Delta E^{r} = -\sum_{i\in A}\sum_{j\in B} C_{ij}^{6} F_{ij}(R_{ij}) R_{ij}^{-6} \tag{3}$$

where

$$F_{ij}(R_{ij}) = \begin{cases} \exp\ [-(1.28R_{ij}^{0}/R_{ij}-1)^{2}], R_{ij} < 1.28R_{ij}^{0}, \\ 1, \quad \text{elsewhere.} \end{cases} \tag{4}$$

R_{ij}^{0} in Eq. (4) is the sum of the van der Waals radii of atoms i and j, and C_{ij}^{6} can be determined from the Slater–Kirkwood relation:

$$C_{ij}^{6} = C_{6}\frac{3}{2}\frac{\alpha_i\alpha_j}{(\alpha_i/N_i)^{1/2}+(\alpha_j/N_j)^{1/2}} \tag{5}$$

α_i and N_i in Eq. (5) denote the atomic polarizability and the number of valence electrons of atoms, respectively. C_6 in Eq. (5) is the only unknown parameter. From our experience [38–41,57], C_6 can be determined in many ways. For example, one could calibrate the incomplete T-model potentials to the properties related to intermolecular interaction energies, such as the second virial coefficients ($B(T)$), the experimental or theoretical dimerization energy. In many cases, C_6 are close to one and the variation within the range of 0.8 and 1.5 does not significantly affect the potential energy surfaces. Since the value of C_6 for similar H-bond systems is 1.43 [38,41], we decided to adopt this value in the present investigation.

2.2. Equilibrium structures in the gas phase

In order to obtain information on the interaction energy surfaces, the computed T-model potentials were applied in the calculations of the equilibrium geometries and interaction energies of the Ala–H_2O and Li^+/Ala–H_2O 1:n complexes, n=1 to 4. The equilibrium geometries in the gas phase could help visualize the three-dimensional arrangements of water molecules in $[Ala]_{aq}$ and $[Li^+/Ala]_{aq}$.

The absolute and local minimum energy geometries of the Ala–H_2O 1:n complexes were computed by placing Ala at the origin of the Cartesian coordinate system. Then, the coordinates of water molecules were randomly generated in the vicinities of Ala. Based on the T-model potentials, the absolute and local minimum energy geometries of the Ala–H_2O 1:n complexes were searched using a minimization technique. Some low-lying minimum energy geometries of the Ala–H_2O 1:1 and 1:2 complexes, which could be important in $[Ala]_{aq}$, are displayed and discussed. In order to sample check the T-model potentials, some of the equilibrium geometries were reoptimized using *ab initio* calculations at the MP2/6–311++G(2d,2p)//MP2/6–311G (d,p) level. In this case, the Berny optimization routine [62] included in Gaussian 98 [60] was employed, by keeping the monomer geometries constant. In order to assess the quality of the basis sets, single-point counterpoise corrections of the Basis Set Superposition Error (BSSE) were made on the optimized geometries. The same procedure was carried out for the Li^+/Ala–H_2O 1:n complexes. Since Li^+ binds strongly with Ala-C in the gas phase, the equilibrium geometry of Li^+/Ala-C could be considered as a supermolecule, in which only the positions and orientations of water molecules were taken into account in *ab initio* geometry optimizations.

2.3. Molecular dynamics simulations

The T-model potentials derived and tested in the previous section were employed in NVE-MD simulations of $[Ala]_{aq}$ and $[Li^+/Ala]_{aq}$. Four sets of MD simulations were performed at 298 K, regarded as MD-$[Ala\text{-}A]_{aq}$, MD-$[Ala\text{-}B]_{aq}$, MD-$[Ala\text{-}C]_{aq}$ and MD-$[Li^+/Ala\text{-}C]_{aq}$. In each MD run, a rigid solute and three hundred water molecules were put in a cubic box subject to periodic boundary conditions [63]. The C–C^{α}–C plane of Ala was coincident with the XY plane of the simulation box, see Fig. 1d to f. The densities of all aqueous solutions were maintained at 1 g/cm^3, corresponding to the box length of 20.9 Å. The cut-off radius was half of the box length. About 50,000 MD steps of 0.0005 ps were devoted to equilibration and additional 100,000 steps to the property calculations. Problems arose when the behavior of water molecules in the first hydration shell of Li^+/Ala-C was to be studied based on pair potentials. Due to the competitive electrostatic interactions among Li^+, H_2O and Ala-C, cares must be exercised in selecting an appropriate model for MD-$[Li^+/Ala\text{-}C]_{aq}$. In order to make our MD simulations possible and reasonable, we decided to simplify the model by considering Li^+/Ala-C as a supermolecule, which was not allowed to move in the course of MD simulations. Since the attractive interaction in the bidentate coordination is stronger than other monodentate coordinations [13,15], our approximated rigid model could represent one of the most probable states in $[Li^+/Ala\text{-}C]_{aq}$.

The most basic one-dimensional views on the structures of $[Ala]_{aq}$ and $[Li^+/Ala]_{aq}$ were obtained from the atom-atom pair correlation functions (g(R)) and the average running coordination number (n(R)). Additionally, in order to characterize and visualize the three-dimensional structures of the H-bond networks in $[Ala]_{aq}$ and $[Li^+/Ala]_{aq}$, the probability distributions maps for the oxygen (PDO) and hydrogen (PDH) atoms of water were constructed from MD simulations [38,39,42]. In the calculations of the PDO and PDH maps, three reference planes were defined with respect to the position and orientation of the solute molecule in the simulation box. They are included in Fig. 1. The volumes above and below the reference planes were divided into layers with the thickness of 1 Å. In each layer, the PDO and PDH maps were computed separately, at the 61×61 grid intersections, by following the trajectories of the oxygen and hydrogen atoms of water in the course of MD simulations. The PDO and PDH maps were represented by contour lines, computed and displayed using the SURFER program [64]. The densities of the contour lines on the PDO and PDH maps are related to the probability of finding the oxygen and hydrogen atoms of water in the aqueous solutions.

Based on a similar approach, some average interaction energy PD maps were constructed from the MD trajectories. The

average solute–solvent and solvent–solvent interaction energy PD maps, regarded as the AWPD and WWPD maps, respectively, were computed and represented by contour lines. The AWPD maps show the average interaction energies between water molecules at the grid intersections and solute, whereas the WWPD maps account for the average interaction energies between water molecules at the grid intersections and all other water molecules in aqueous solution. Only negative interaction energies are displayed on the maps.

In order to visualize the total–average potential energy landscapes, as well as to provide basic energetic information to characterize the dynamics of water molecules in the H-bond networks, the total–average interaction energy PD (AW-WWPD) maps were constructed by combination of the AWPD and WWPD maps [38,39,42]. The structures of the AWPD, WWPD and AW-WWPD maps were examined in details using cross section plots [38,39], generated by taking vertical slices along predefined profile lines on their surfaces. The cross section plots derived from the longitudinal profile lines could be associated with the average potential energy barriers to the diffusion of water molecules within and between the H-bond networks ($\langle \Delta E_{aq}^{L} \rangle$), whereas those obtained from the transverse profile lines could be attributed to the average potential energy barriers to the diffusion of water molecules between the H-bond networks and the outside ($\langle \Delta E_{aq}^{T} \rangle$). $\langle \Delta E_{aq}^{L} \rangle$ and $\langle \Delta E_{aq}^{T} \rangle$ are considered to be part of the average potential energy channel for the diffusion of water molecule in the H-bond network.

Attempt was further made to obtain information on the water exchange processes at the H-bond networks of the solutes. Although not straightforward, we have shown that the dynamics of specific water molecules in the first hydration shells of solute, such as the longest H-bond lifetime ($\tau_{A-H...Ow,max}$), could be anticipated at least qualitatively from the structures of the total–average potential energy landscapes [38,39]. Additionally, in the present case, the water exchange diagrams [43,44], showing the distance between a specific water molecule and a functional group of solute as a function of MD simulation time, were constructed, from which the water residence times at Li^+ ($\tau_{Li^+...Ow}$) and the H-bond lifetimes ($\tau_{A-H...Ow}$) at the functional groups were approximated. The lifetimes of the water exchange intermediate complexes at Li^+ and at the H-bonds, denoted by $\tau_{ex,Li^+...Ow}$ and $\tau_{ex,A-H...Ow}$, respectively, were determined from the analysis of the water exchange diagrams. The five-water exchange pathways proposed by Langford and Gray [65] were tentatively employed in the analysis of the water exchange processes. They have been applied successfully, for example, in $[Li^+]_{aq}$ [43,44] and $[Na^+]_{aq}$ [43]. In the course of MD simulations, the total interaction energies (ΔE^{AW-WW}) of selected water molecules were recorded and included in the water exchange diagrams.

3. Results and discussion

3.1. Equilibrium structures in the gas phase

Some absolute and low-lying minimum energy geometries for the Ala-A–H_2O, Ala-B–H_2O, Ala-C–H_2O and Li^+/Ala-C–H_2O 1:*n* complexes, computed from the T-model potentials, are illustrated in Figs. 2–5. $\Delta E_{T\text{-model}}$ and some characteristic distances and angles, together with the corresponding MP2 results, are included in the figures.

3.2. The Ala–H_2O complex

The absolute minimum energy geometry of the Ala-A–H_2O 1:1 complex, obtained from the T-model potential, is structure a in Fig. 2. Structure a consists of a cyclic H-bond, in which water acts simultaneously as proton donor and acceptor towards the C=O1 and O2–H7 groups, respectively. This type of cyclic H-bond has been commonly found in R–COOH–H_2O 1:1 complexes [40,51]. $\Delta E_{T\text{-model}}$ of structure a is −41.4 kJ/mol, with the Ow–Hw···O1 and O2–H7···Ow H-bond distances of 2.93 and 2.85 Å, respectively. MP2/6–311++G(2d,2p)//MP2/6–311G(d,p) geometry optimization predicted the same structure, with slightly shorter Ow–Hw···O1 and O2–H7···Ow H-bond distances. ΔE_{MP2} and ΔE_{MP2CP} of structure a in Fig. 2 are −41.4 and −34.3 kJ/mol, respectively. *Ab initio* calculations at the HF/6–31G(d,p) [66] and MP2/6–311++G(d,p) [51] levels suggested the same equilibrium geometry. The Ow–Hw···O1 and O2–H7···Ow H-bond distances computed at the HF level are 2.78 and 2.67 Å, respectively.

The second and third low-lying minimum energy geometries of the Ala-A–H_2O 1:1 complex are represented by a cyclic H-bond, in which water molecule acts simultaneously as proton donor towards the C=O1 group and proton acceptor towards the N–H3 and N–H2 groups, respectively. $\Delta E_{T\text{-model}}$ of structures b and c are almost identical, −29.3 and −29.1 kJ/mol, respectively. The N–H3···Ow and Ow–Hw···O1 H-bond distances in structure b are 3.04 and 2.99 Å, respectively, whereas the N–H2···Ow and Ow–Hw···O1 H-bond distances in structure c are 3.11 and 2.95 Å, respectively. MP2/6–311++G(2d,2p)//MP2/6–311G(d,p) calculations suggested that structure c is slightly more stable than structure b. Three low-lying minimum energy geometries of the Ala-B–H_2O 1:1 complex, obtained from the T-model potential, are structures d, e and f in Fig. 2. The H-bond structure at the COOH group seems not affected when the angle ϕ of Ala was rotated 30° about the N–C^{α} bond. The H-bonding feature in structure d is almost identical to structure a, with the same interaction energy. The 30° rotation of the N–C^{α} bond seems to bring about more visible effects to the N–H...Ow H-bonds; the interaction energy in structure e is slightly higher than structure b, whereas that of structure f is about 4 kJ/mol higher than structure c.

For the Ala-C–H_2O 1:1 complex, the cyclic H-bond in structure g is nearly identical to those in structures a and d. From chemical intuitions, one could expect that the N and O1 atoms in Ala-C might act simultaneously as proton acceptors towards both O–H groups of water molecule. In the present case, however, the approach of only one O–H group towards both N and O1 atoms was found in structures h and i, with the interaction energies of about −30 kJ/mol. Although this type of interaction is not very common, it was observed in protein crystals [67] and has been regarded as a bifurcated or three-center H-bond [68]. The term has been used to describe the situation, in which a single proton is shared between two H-

bond acceptors. They were found, for example, in β-sheet structures of carboxypeptidase [55].

Since the characteristic structures of H-bonds in the Ala-B–H_2O and Ala-C–H_2O 1:2 complexes are similar to the Ala-A–H_2O 1:2 complexes, only some results on the latter are discussed. The lowest-lying minimum energy geometry for the Ala-A–H_2O 1:2 complex is structure a in Fig. 3. For structure a, both water molecules act as proton donor and acceptor toward the COOH

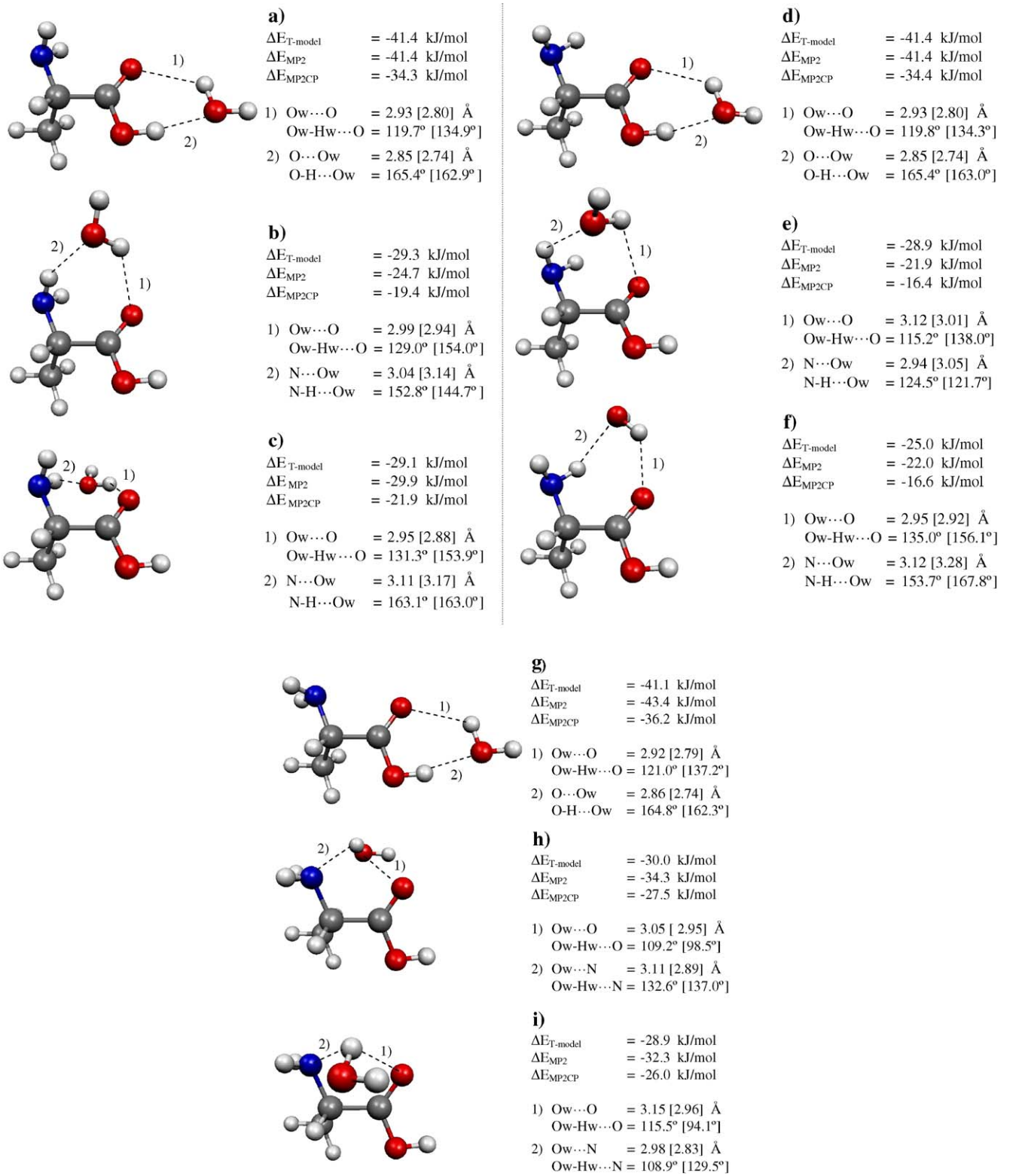

Fig. 2. Equilibrium structures, interaction energies and some characteristic H-bond distances and angles of the Ala–H_2O 1:1 complexes in the gas phase, computed from the T-model potentials and MP2 calculations. (a–c) Ala-A–H_2O 1:1 complexes, (d–f) Ala-B–H_2O 1:1 complexes, (g–i) Ala-C–H_2O 1:1 complexes. MP2CP=MP2 calculations with single-point counterpoise correction. […]=values obtained from MP2/6–311G(d,p).

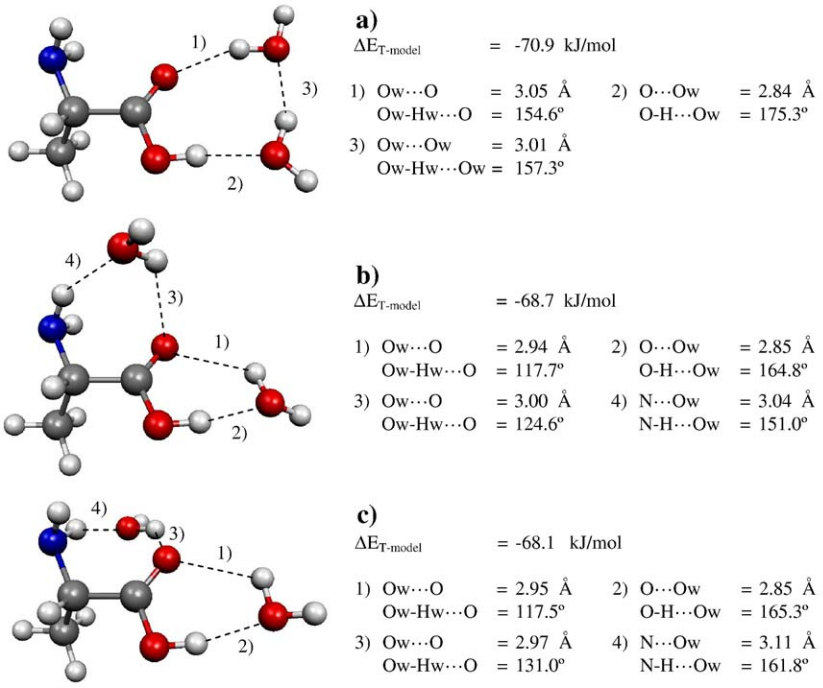

Fig. 3. Equilibrium structures, interaction energies and some characteristic H-bond distances and angles of the Ala-A–H_2O 1:2 complexes in the gas phase, computed from the T-model potentials.

group, forming a larger cyclic H-bond structure. $\Delta E_{\text{T-model}}$ of structure a is −70.9 kJ/mol, with the Ow–Hw···O1 and O2–H7···Ow H-bond distances of 3.05 and 2.84 Å, respectively. Structures b and c in Fig. 3 consist of two cyclic H-bonds, with the H-bond structures similar to those in the Ala-A–H_2O 1:1 complexes. Structures b and c possess comparable interaction energies. They are slightly higher than structure a. The structures of the Ala-A–H_2O 1:2 complexes derived from the T-model potentials agree in general with those reported in Ref. [51], in which the results of *ab initio* calculations with larger basis set on the Ala–H_2O 1:*n* complexes, with $n=1$ to 2, were reported.

3.3. The Li^+/Ala–H_2O complex

The T-model and MP2 results on the Li^+/Ala-C–H_2O complexes are displayed in Fig. 4. Fig. 4a shows the equilibrium geometry of Li^+/Ala-C computed from MP2/6–311++G(2d,2p) calculations; the Li^+…O and Li^+…N distances are 1.92 and 2.08 Å, respectively, with ΔE_{MP2} of −261.1 kJ/mol. The Li^+…O and Li^+…N distances, as well as the binding energy, are comparable with those computed from B3LYP/6–311++G(d,p) calculations [13], 1.86 Å, 2.05 Å and −248.3 kJ/mol, respectively.

The bidentate coordination of Li^+ at the N and O1 atoms of Ala-C brings about significant effects at the COOH and NH_2 groups. Both T-model and MP2 calculations suggested structure b, in which water molecule binds directly at Li^+, to be the most favorable form of the Li^+/Ala-C–H_2O 1:1 complex, with $\Delta E_{\text{T-model}}$ and ΔE_{MP2} of −97.3 and −105.0 kJ/mol, respectively. The bidentate coordination directly affects the O2–H7…Ow H-bond structure and interaction energy. Structure c in Fig. 4 consists of a linear O2–H7…Ow H-bond, compared to a cyclic H-bond in the Ala-C–H_2O 1:1 complex, structure g in Fig. 2. The binding of Li^+ to Ala-C leads to an increase in the stability of the O2–H7…Ow H-bond, between 18 and 13 kJ/mol depending on the method used. Structures d and e in Fig. 4 show the N–H2…Ow and N–H3…Ow H-bonds, which are also stabilized by the bidentate coordination of Li^+, with $\Delta E_{\text{T-model}}$ of about −50 kJ/mol. Similar results were obtained for the Li^+/Ala-C–H_2O 1:2, 1:3 and 1:4 complexes, shown in Fig. 5, in which additional water molecule prefers to bind directly at Li^+, and subsequently at the O2–H7 and N–H2 groups. It appeared that, in the gas phase, not more than two water molecules can directly hydrate at Li^+, compared to four in the case of the Li^+/H_2O complex [69]. This is in good agreement with the theoretical results obtained from B3LYP/6–311++G(d,p) and MP2/6–311++G(d,p) calculations, as well as experiment on the Li^+/Val–H_2O 1:2 and 1:3 complexes, in which only two water molecules interact solely at Li^+ and the third one at Val molecule [10].

Based on the results summarized in this section, one can conclude that the T-model potentials predicted reasonable gas-phase equilibrium structures and interaction energies for all the Ala–H_2O and Li^+/Ala-C–H_2O 1:*n* complexes considered. They can be further applied in MD simulations of the aqueous solutions with confidence.

3.4. MD simulations

In order to limit the number of figures, only selected g(R), PDO and AW-WWPD maps, together with their cross section plots, are displayed and used in the discussion. Characteristic high-density contours on the PD maps are labeled with letters: A at the O2–H7 group; B and C at the lone-pair electrons of O1, above and below the COOH plane, respectively; D and E at H3 and H2, respectively; F at the C1–H1 group; and G at the CH_3

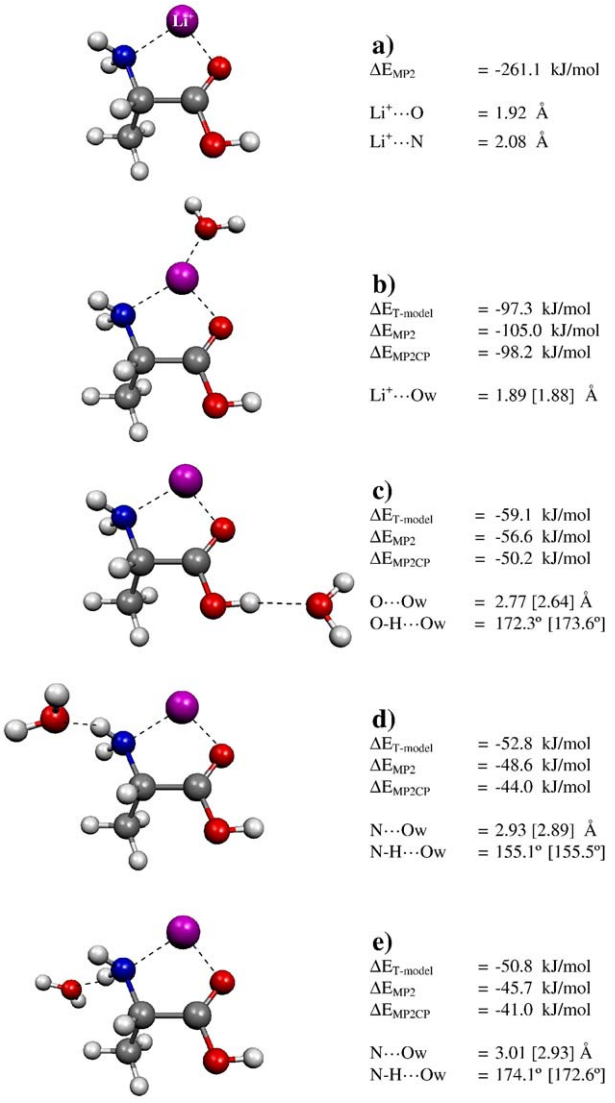

Fig. 4. Equilibrium structures, interaction energies and some characteristic distances and angles in the Li^+/Ala-C and Li^+/Ala-C–H_2O complexes in the gas phase, computed from the T-model potentials and MP2 calculations. (a) Li^+/Ala-C complex, (b–e) Li^+/Ala-C–H_2O 1:1 complexes. MP2CP=MP2 calculations with single-point counterpoise correction. […]=values obtained from MP2/6–311G(d,p).

group. They represent the H-bond networks of water in the first hydration shells of Ala. In order to compare the average potential energy barriers to the diffusion of water molecules ($\langle \Delta E_{aq}^{L} \rangle$ and $\langle \Delta E_{aq}^{T} \rangle$) in the H-bond networks, the lowest energy minima in the cross section plots were set to zero.

3.5. $[Ala]_{aq}$

Since the structures of Ala-A and Ala-B are different only at the NH_2 group, one could expect that the structures and peak positions of g(R) for the COOH group are not substantially different. This is confirmed by the results in Fig. 6a to d. For both $[Ala\text{-}A]_{aq}$ and $[Ala\text{-}B]_{aq}$, the positions of the main peaks of $g(R_{O2...Ow})$ are seen at 2.91 Å. The integrations of $g(R_{O2...Ow})$ to these peak positions suggested a little more than one water molecule (1.31 and 1.23, respectively) H-bonding directly at the O2–H7 group, which is compared well with 1.4 in the case of $[BA]_{aq}$ [40]. It should be noted that larger number of water molecule in close contact with the O2–H7 group in $[Ala\text{-}A]_{aq}$ does not necessarily mean that the O2–H7…Ow H-bond is stronger than in $[Ala\text{-}B]_{aq}$. To resolve this ambiguity, the results on $g(R_{O2...Ow})$ have to be supplemented by the PDO maps. The O2–H7…Ow H-bond corresponds to the H-bond networks labeled with A on the PDO maps in Fig. 7a, d, f and i. The contour density at A in $[Ala\text{-}B]_{aq}$ is higher than in $[Ala\text{-}A]_{aq}$, implying an increase in the degree of hydration at A upon the N–C^{α} bond rotation. For $[Ala\text{-}A]_{aq}$ and $[Ala\text{-}B]_{aq}$, the main peaks of $g(R_{O1...Ow})$ are seen at 3.11 and 3.16 Å, respectively, with about two water molecules (1.97 and 2.33, respectively) in close contact with O1. The two water molecules act as proton donor towards the lone-pair electrons of O1 and correspond to the H-bond networks labeled with B and C in Fig. 7a, b and e for $[Ala\text{-}A]_{aq}$, and Fig. 7f, g and j for $[Ala\text{-}B]_{aq}$. The contour densities at B and C in $[Ala\text{-}B]_{aq}$ are a little lower than in $[Ala\text{-}A]_{aq}$.

For $[Ala\text{-}A]_{aq}$, the position of the main peak of $g(R_{N...Ow})$ is located at 3.16 Å, with approximately two (1.92) water molecules H-bonding with both N–H groups. They are labeled with D and E and clearly seen on the PDO maps in Fig. 7a to c. Since H2 and H3 are in different environment, due to the presence of the CH_3 group adjacent to H2, the structures of $g(R_{H2...Ow})$ and $g(R_{H3...Ow})$ in Fig. 6b are quite different, for which the main peak of $g(R_{H2...Ow})$ is more structured than $g(R_{H3...Ow})$. This suggests that the N–H2…Ow H-bond could be more associated than the N–H3…Ow H-bond, in line with the PDO maps in Fig. 7c, in which a more well defined H-bond network at E compared to D is evident. The degree of hydration at the NH_2 group seems to be decreased when the angle ϕ varies from 0° to 30°. For $[Ala\text{-}B]_{aq}$, the main peak of $g(R_{N...Ow})$ in Fig. 6d is located at 3.11 Å, with lower number of water molecules (1.54) in close contact with both N–H groups compared to $[Ala\text{-}A]_{aq}$. Moreover, the main peak of $g(R_{H2...Ow})$ in Fig. 6d possesses nearly no structure, another indicator for a weaker N–H2…Ow H-bond upon the rotation. Comparison of the PDO maps in Fig. 7c and h also shows decreases in the contour densities at D and E, due to the rotation of the N–C^{α} bond. This confirms the results of $g(R_{N...Ow})$. The decrease in the degree of hydration at the NH_2 groups seems to be accompanied by an increase in the contour density at F, which means that the H-bond network at the C1–H1 group becomes stronger upon rotation; since in Ala-B, H3 is closer to H1, and the H-bond networks nearby can partly overlap.

The structures and peak positions of g(R) for the COOH group are slightly modified when the angle ϕ is rotated 180° about the N–C^{α} bond. For $[Ala\text{-}C]_{aq}$, the main peak of $g(R_{O1...Ow})$ in Fig. 6e is seen at 3.11 Å, with approximately two (1.84) water molecules in close contact with the C=O1 group. $g(R_{O2...Ow})$ in Fig. 6 shows that the number of water molecules in close contact with the O2–H7 group is not much affected when the angle ϕ varies from 0° to 30° to 180°, respectively. However, an increase in the degree of hydration at the O2–H7 group is more evident from the PDO maps, on which the contour density at A in $[Ala\text{-}C]_{aq}$ is a little higher

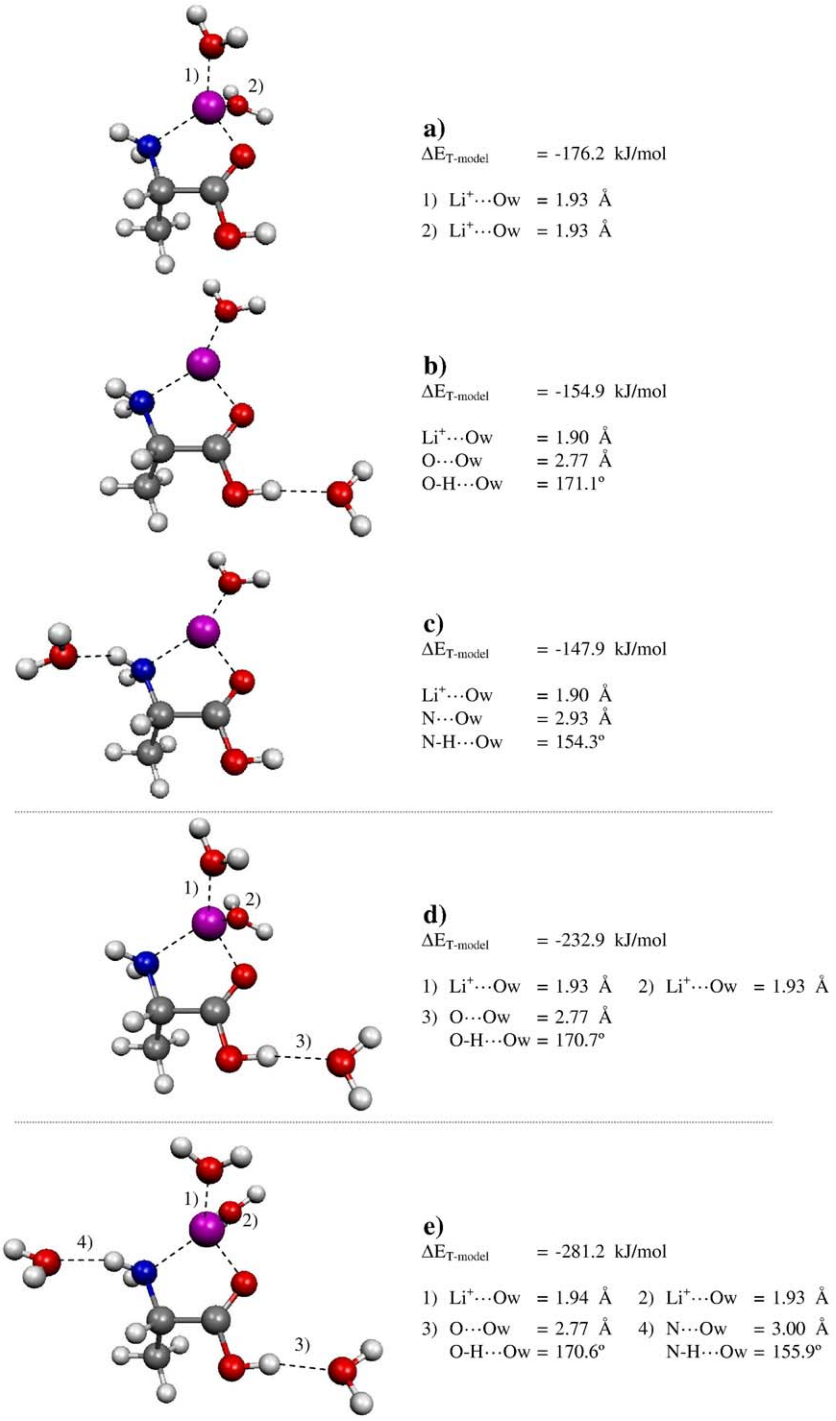

Fig. 5. Equilibrium structures, interaction energies and some characteristic distances and angles in the Li^+/Ala-C–H_2O complexes in the gas phase, computed from the T-model potentials. (a–c) Li^+/Ala-C–H_2O 1:2 complexes, (d) Li^+/Ala-C–H_2O 1:3 complex, (e) Li^+/Ala-C–H_2O 1:4 complex.

than in $[Ala\text{-}B]_{aq}$ and in $[Ala\text{-}A]_{aq}$, respectively. The structures of the main peaks of $g(R_{H2\ldots Ow})$ and $g(R_{H3\ldots Ow})$ in Fig. 6f are roughly the same as in Fig. 6d. They confirm that the variation of the angle ϕ from 0° to 30° to 180° destabilizes the H-bond networks at the NH_2 groups. The 180° rotation of the NH_2 group creates an additional well defined H-bond network, labeled with I in Fig. 7n. This H-bond network is adjacent to F, spanning from H1 to the nearest H atom of the CH_3 group. The PDO maps also reveal a small H-bond network in the area between the N and O1 atoms in Ala-C, labeled with H in Fig. 7k to m and o. This H-bond network seems to be an evidence showing the existence of the bifurcated H-bond, in which a water molecule acts as a proton donor towards both N and O1 atoms of Ala-C, see structure h and i in Fig. 2.

The effects of conformation change on the hydration dynamics in $[Ala\text{-}A]_{aq}$, $[Ala\text{-}B]_{aq}$ and $[Ala\text{-}C]_{aq}$ are discussed in the first place using the cross section plots in Fig. 8 and $\tau_{A-H..B,\ max}$ in Table 1. Since, on the PDO maps, the H-bond networks at A are

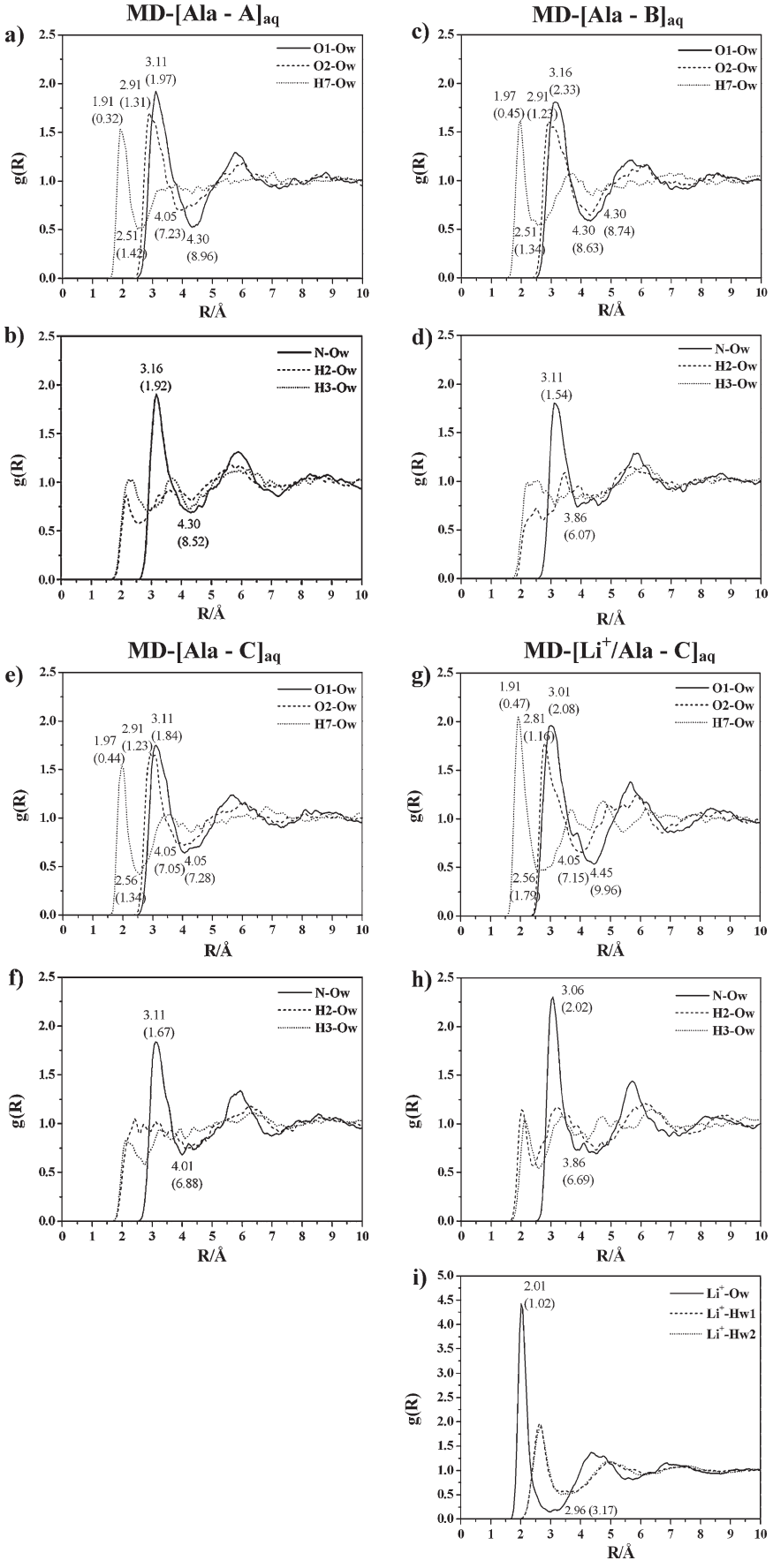

Fig. 6. g(R) obtained from MD simulations at 298 K. Some characteristic distances are shown, with the average running coordination number (n(R)) in parenthesis. (a–b) MD-[Ala-A]$_{aq}$, (c–d) MD-[Ala-B]$_{aq}$, (e–f) MD-[Ala-C]$_{aq}$, (g–i) MD-[Li^+/Ala-C]$_{aq}$.

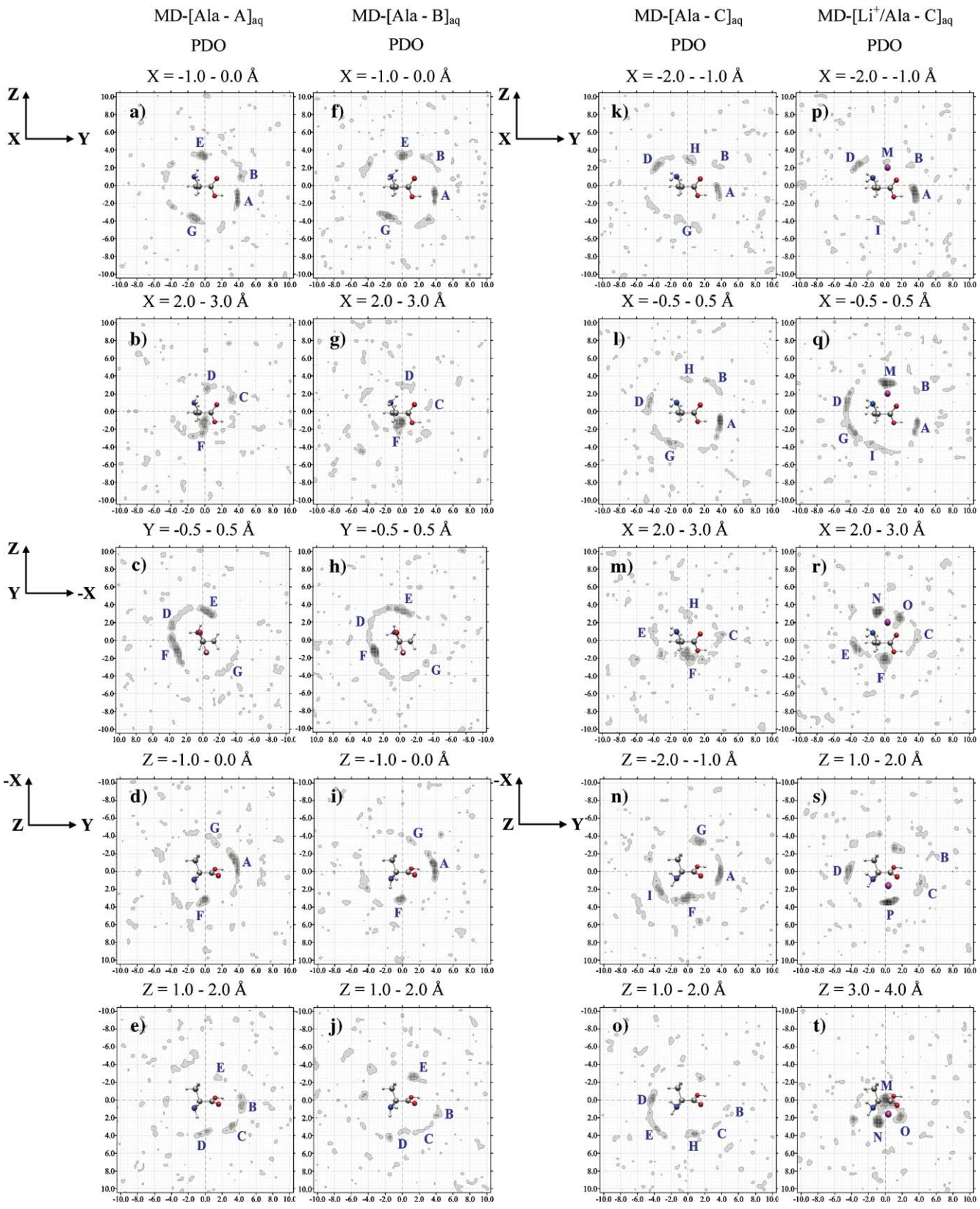

Fig. 7. Some PDO maps obtained from MD simulations at 298 K. (a–e) MD-[Ala-A]$_{aq}$, (f–j) MD-[Ala-B]$_{aq}$, (k–o) MD-[Ala-C]$_{aq}$, (p–t) MD-[Li^+/Ala-C]$_{aq}$.

the most well defined, attention is focused on the behavior of water molecules forming H-bonds with the O2–H7 group. Selected water exchange diagrams are displayed in Fig. 9, together with the corresponding ΔE^{AW-WW}. The low-pass filter [70] was employed to smooth all the data plots in Fig. 9. Some representative results of $\tau_{O2-H7...Ow}$ and $\tau_{ex,O2-H7...Ow}$, together

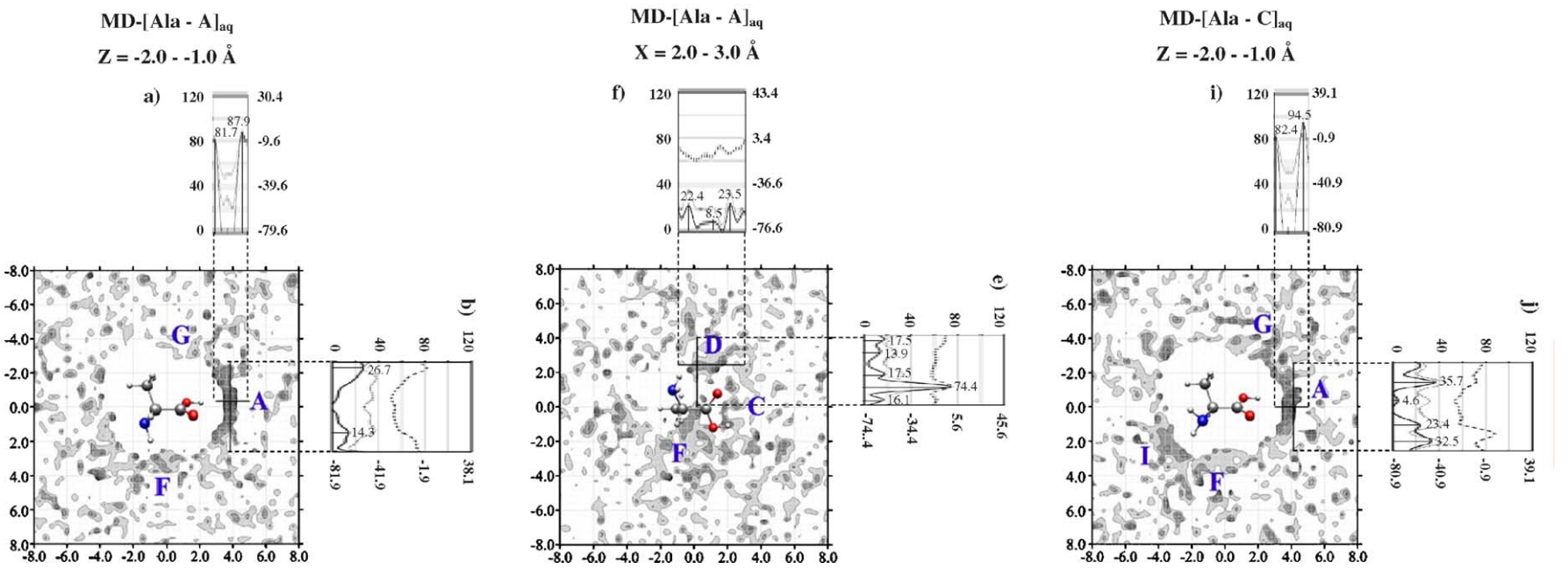

Fig. 8. Selected AW-WWPD maps and the corresponding cross section plots obtained from the transverse and longitudinal profile lines. (———) The total–average interaction energy. (– – – – – –) The average solute–solvent interaction energy. (- - - - -) The average solvent–solvent interaction energy. Energy values and distances are in kJ/mol and Å, respectively. The lowest energy minima on the cross section plots are set to zero to show the average potential energy barriers for the motion of water molecule.

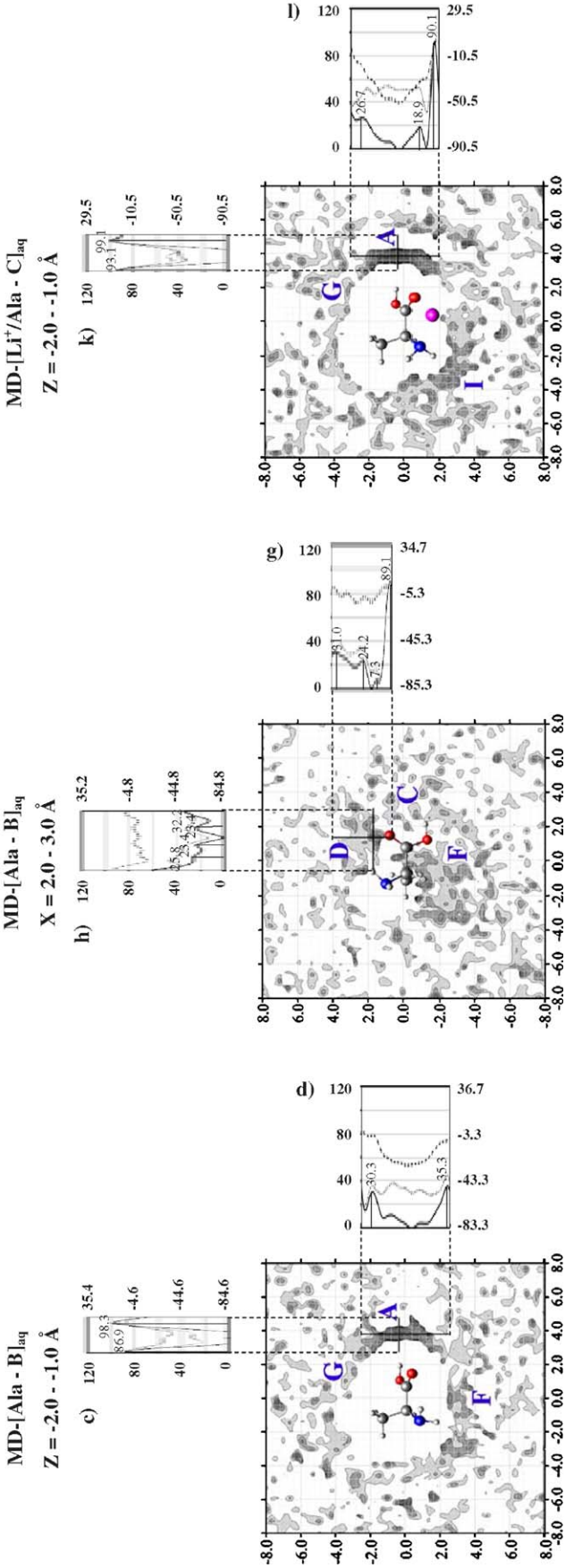

Fig. 8 (*continued*).

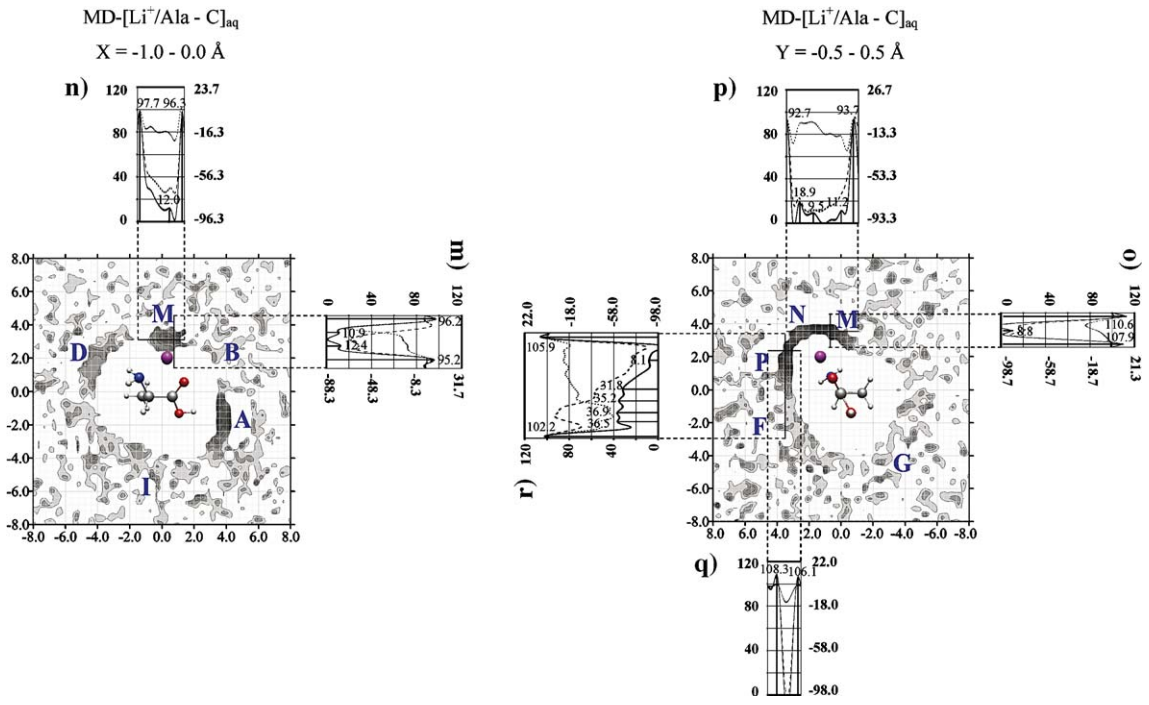

Fig. 8 (*continued*).

with the water exchange pathways obtained from the analysis of the water exchange diagrams, are listed in Table 2. The energetic paths of the water exchange processes were explored by calculations of the activation interaction energy of the transition state complex (ΔEa^{AW-WW}), defined as the difference between the average interaction energy of a specific water molecule in the first hydration shell (ΔE_{av}^{AW-WW}) and its interaction energy at the water exchange transition state (ΔE_{TS}^{AW-WW}). These energy values can be extracted from the water exchange diagrams and some of them are given in Table 2. The derivations of ΔEa^{AW-WW}, as well as $\tau_{A-H...Ow}$ and $\tau_{ex,A-H...Ow}$, are also shown in Table 2. Attempt was further made to establish correlations among these energies and times. Some meaningful results are displayed in Fig. 10.

Comparisons among the cross section plots in Fig. 8a to d and i and j show that the rotation of the N–C^{α} bond from the angle $\phi = 0°$ to 30° to 180° leads to visible effects on the total–average potential energy landscapes at A, especially in $[Ala\text{-}C]_{aq}$ compared to $[Ala\text{-}A]_{aq}$ and $[Ala\text{-}B]_{aq}$. For $[Ala\text{-}C]_{aq}$, the cross section plot derived from the longitudinal profile line in Fig. 8j shows more structures compared to the others. This could reduce the mobility of water molecule inside the H-bond network at A in $[Ala\text{-}C]_{aq}$, compared to $[Ala\text{-}A]_{aq}$ and $[Ala\text{-}B]_{aq}$. Since $\langle \Delta E_{aq}^{T} \rangle$ could be correlated with $\tau_{A-H...B,max}$ [38,39], one anticipates from the values of $\langle \Delta E_{aq}^{T} \rangle$ in Fig. 8a, c and i that $\tau_{O2-H7...Ow,max}$ in $[Ala\text{-}B]_{aq}$ is larger than $[Ala\text{-}C]_{aq}$ and $[Ala\text{-}A]_{aq}$, respectively. The values of $\tau_{O2-H7...Ow,max}$ in Table 1 confirm this anticipation namely, $\tau_{O2-H7...Ow,max}$ in $[Ala\text{-}B]_{aq}$, $[Ala\text{-}C]_{aq}$ and $[Ala\text{-}A]_{aq}$ are 21.2, 20.4 and 19.6 ps, respectively. By application of a simple relationship between the water exchange rate constant (k_{ex}) and the water residence time (τ_{res}) ($k_{ex} = 1/\tau_{res}$) [44], k_{ex} at the O2–H7 groups in $[Ala\text{-}B]_{aq}$, $[Ala\text{-}C]_{aq}$ and $[Ala\text{-}A]_{aq}$ are 47.2 and 49.1 and 50.9 ns^{-1}, respectively. A similar conclusion could be made for the H-bond networks at the NH_2 group, in which $\langle \Delta E_{aq}^{T} \rangle$ at D in $[Ala\text{-}B]_{aq}$ is a little higher than $[Ala\text{-}A]_{aq}$, resulting in longer $\tau_{N-H3...Ow,max}$ in $[Ala\text{-}B]_{aq}$, see Fig. 8e and g, as well as Table 1. $\tau_{N-H3...Ow,max}$ in $[Ala\text{-}B]_{aq}$ and $[Ala\text{-}A]_{aq}$ are 16.2 and 13.1 ps, respectively, corresponding to k_{ex} at the N–H3 groups of 61.5 and 76.2 ns^{-1}, respectively.

Since the water residence times or the H-bond lifetimes are sensitive to the definitions and methods employed in the investigations, and the values in the literatures vary in a wide range. Therefore, care must be exercised in comparison the present results with the others. The longest H-bond lifetimes reported here could be compared in the first place with our results

Table 1
The longest H-bond lifetimes ($\tau_{A-H\cdots Ow,max}$) and the longest water residence times ($\tau_{Li^+\cdots Ow,\,max}$), together with the water exchange rate constants ($k_{ex,\,A-H\cdots Ow}$ and $k_{ex,\,Li^+\cdots Ow}$) obtained from MD simulations of $[Ala]_{aq}$ and $[Li^+/Ala]_{aq}$, respectively

MD	O2–H7···Ow		N–H···Ow		Li^+···Ow	
	$\tau_{O2-H7\cdots Ow,max}$	$k_{ex,O2-H7\cdots Ow}$	$\tau_{N-H\cdots Ow,max}$	$k_{ex,N-H\cdots Ow}$	$\tau_{Li^+\cdots Ow,max}$	$k_{ex,Li^+\cdots Ow}$
$[Ala\text{-}A]_{aq}$	19.63	50.9	13.12	76.2	–	–
$[Ala\text{-}B]_{aq}$	21.17	47.2	16.25	61.5	–	–
$[Ala\text{-}C]_{aq}$	20.37	49.1	17.19	58.2	–	–
$[Li^+/Ala\text{-}C]_{aq}$	28.03	35.7	17.99	55.6	38.02	26.3

Time in ps and rate constant in ns^{-1}.

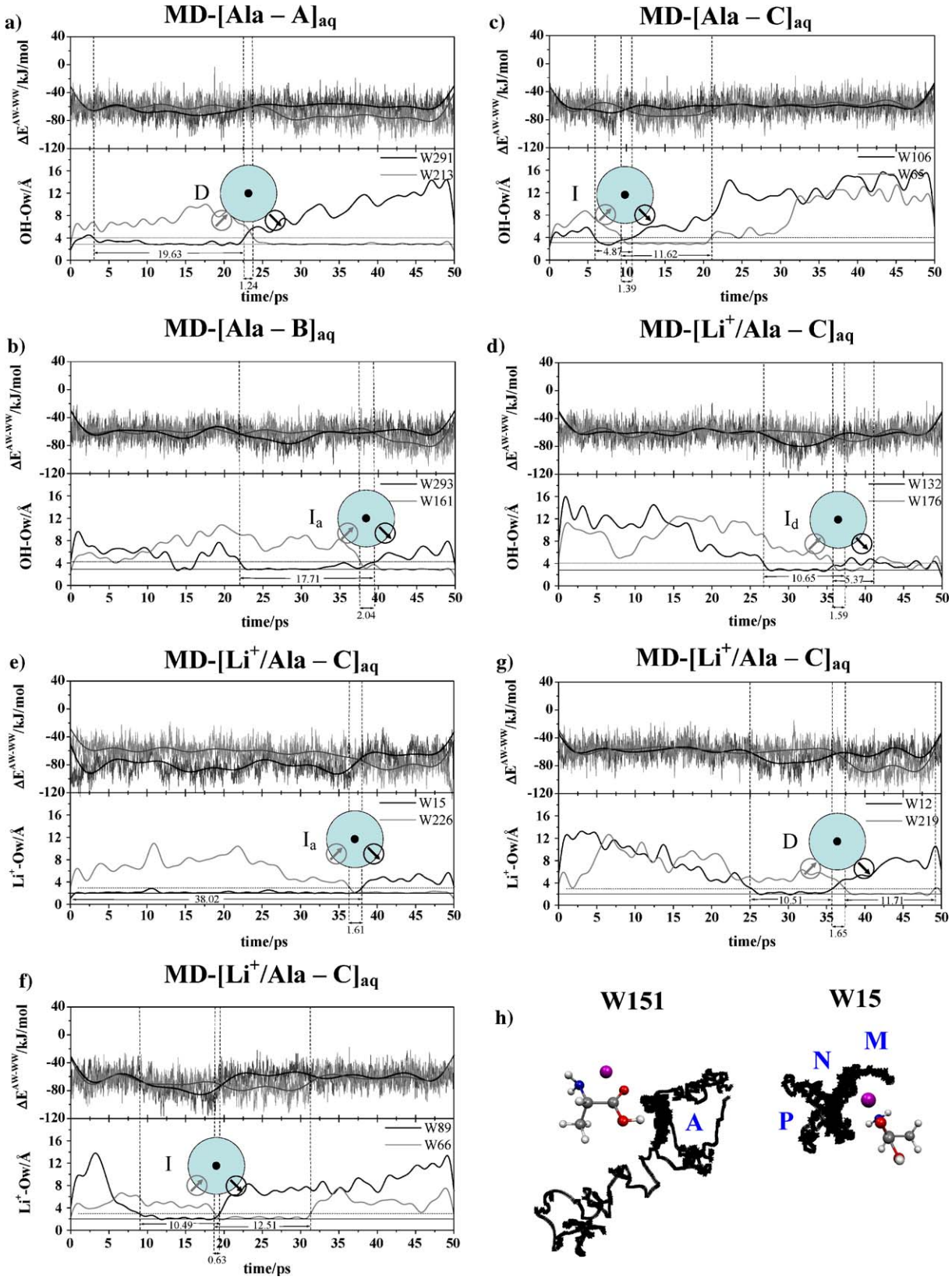

Fig. 9. Selected water exchange diagrams for specific water molecule in the first hydration shell of the O2–H7 group and Li^+, together with the corresponding total interaction energy (ΔE^{AW-WW}) monitored in course of MD simulations. Some water exchange mechanisms proposed by Langford and Gray [65] are also included in the figure. (a–d) At the O2–H7 groups in $[Ala\text{-}A]_{aq}$, $[Ala\text{-}B]_{aq}$, $[Ala\text{-}C]_{aq}$ and $[Li^+/Ala\text{-}C]_{aq}$, respectively. (e–g) At Li^+ in $[Li^+/Ala\text{-}C]_{aq}$. (h) Selected trajectories of water molecules at the O2–H7 group and Li^+ obtained from MD-$[Li^+/Ala\text{-}C]_{aq}$, denoted by W151 and W15, respectively.

Table 2
The results extracted from the water exchange diagrams, together with the derivation of $\tau_{A-H\cdots Ow}$, τ_{ex} and ΔEa^{AW-WW}

(a) O2–H7···Ow

Mechanism[a]	Water molecule A $\tau_{O2-H7\cdots Ow}$	$\tau_{ex,O2-H7\cdots Ow}$	Water molecule B $\tau_{O2-H7\cdots Ow}$	ΔEa^{AW-WW}
MD-[Ala-A]$_{aq}$				
I_a	7.50	0.87	–	–
I	17.39	1.59	7.50	–
I_d	15.98	0.11	6.04	–
D	19.63	1.24	–	7.8
D	16.30	0.13	8.67	5.2
MD-[Ala-B]$_{aq}$				
I_a	17.71	2.04	–	6.4
I_a	8.29	0.89	4.73	–
I	16.67	0.79	8.30	–
I_d	3.50	1.23	21.17	–
I_d	15.17	0.45	9.11	–
D	3.78	1.20	5.31	–
D	3.37	0.72	8.29	–
MD-[Ala-C]$_{aq}$				
I_a	7.87	1.62	7.39	5.3
I_a	11.63	1.15	20.37	3.7
I_a	6.41	0.64	5.65	5.5
I	4.87	1.39	11.62	2.3
I_d	5.65	0.38	4.25	–
MD-[Li$^+$/Ala-C]$_{aq}$				
I_a	24.65	1.03	5.37	5.3
I_a	–	1.35	6.23	–
I	28.02	1.91	–	10.3
I	–	0.77	28.02	–
I_d	5.65	1.64	10.65	–
I_d	10.65	1.59	5.37	6.3
I_d	8.87	0.37	4.51	–
I_d	3.73	0.25	5.37	–
D	11.89	0.36	10.65	–
D	8.01	0.09	–	–

(b) Li$^+$···Ow

Mechanism	Water molecule A $\tau_{Li^+\cdots Ow}$	$\tau_{exLi^+\cdots Ow}$	Water molecule B $\tau_{Li^+\cdots Ow}$	ΔEa^{AW-WW}
MD-[Li$^+$/Ala-C]$_{aq}$				
I_a	38.02	1.61	–	8.4
I_a	12.33	1.32	14.51	11.5
I	10.49	0.63	12.51	5.8
D	10.51	1.65	11.71	10.0

MD simulation times in ps and energies in kJ/mol.

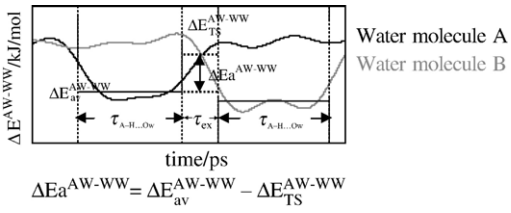

$\tau_{O2-H7\cdots Ow}$ = H-bond residence time at the O2–H7 group.
$\tau_{Li^+\cdots Ow}$ = water residence time at Li$^+$.
$\tau_{ex,O2-H7\cdots Ow}$ = lifetime of the water exchange intermediate complex at the O2–H7 group.
$\tau_{ex,Li^+\cdots Ow}$ = lifetime of the water exchange intermediate complex at Li$^+$.

in $[H_2O]_{aq}$ [39] and $[Alaz]_{aq}$ [38]. $\tau_{Ow-Hw\ldots Ow,max}$ in $[H_2O]_{aq}$ is 8.7 ps, whereas $\tau_{N-H\ldots Ow,max}$ at the NH_3^+ group and $\tau_{Ow-Hw\ldots O,max}$ at the COO^- group in $[Alaz]_{aq}$ are 21.3 ps and 5.1 ps, respectively. The longest H-bond lifetimes reported in the present and previous work [38,39] are also quite reasonable, compared with the water residence times ($\langle\tau_{rt}\rangle$) obtained from MD simulations of the bovine pancreatic trypsin inhibitor (BPTI) in aqueous solution [34], in which $\langle\tau_{rt}\rangle$ in $[H_2O]_{aq}$, at the amide protons (SC_HN) of asparagine (Asn) and at the hydroxyl proton (SC_HO) of serine (Ser) are approximately 10, 22 and 49 ps, respectively. In other words, the water residence time in pure water is smaller than at the N–H and O–H groups of proteins, respectively; which agrees qualitatively well with our results.

The water residence times and the water exchange mechanisms in $[Ala\text{-}A]_{aq}$, $[Ala\text{-}B]_{aq}$ and $[Ala\text{-}C]_{aq}$ could be further discussed in details using the water exchange diagrams in Fig. 9a to c and the results in Table 2a. We are aware of the fact that, due to the complexity of the solute structures, the water exchange mechanisms in $[Ala\text{-}A]_{aq}$, $[Ala\text{-}B]_{aq}$ and $[Ala\text{-}C]_{aq}$ cannot be exactly the same as those in $[Li^+]_{aq}$ [43,44] and $[Na^+]_{aq}$ [43]. However, to simplify the discussion, we decided to restrict ourselves primarily to the five-water exchange mechanisms proposed by Langford and Gray [65], namely, the dissociative (D), associative (A) and interchange (I) mechanisms; the I mechanism could be subdivided into two classes, depending on whether the interchange is associative-like or dissociative-like, regarded as I_a and I_d mechanisms, respectively. Fig. 9a to c show some predominant water exchange processes at the O2–H7 group of $[Ala\text{-}A]_{aq}$, $[Ala\text{-}B]_{aq}$ and $[Ala\text{-}C]_{aq}$. It appeared from the analysis of the water exchange diagrams that, at the COOH groups, the I mechanisms are more favored than the D mechanism, with $\tau_{O2-H7\ldots Ow}$ and $\tau_{ex,O2-H7\ldots Ow}$ varying in quite wide ranges. The former is from 3.4 to 21.2 ps and the latter from 0.1 to 2.0 ps. Weak correlations were established between $\tau_{O2-H7\ldots Ow}$ and ΔEa^{AW-WW}, as well as $\tau_{ex,O2-H7\ldots Ow}$ and ΔE^{AW-WW}. The trends of the correlation plots in Fig. 10a and b support the anticipation made from the total–average potential energy landscapes and the cross section plots namely, the higher ΔEa^{AW-WW} the longer $\tau_{O2-H7\ldots Ow}$ and $\tau_{ex,O2-H7\ldots Ow}$.

3.6. $[Li^+/Ala]_{aq}$

Since one of our main objectives is to investigate the effects of Li^+ on the H-bond networks of water in the first hydration shell of Ala, the discussion in the present section will be made based on the results of MD-$[Ala\text{-}C]_{aq}$ and MD-$[Li^+/Ala\text{-}C]_{aq}$. g(R) obtained from MD-$[Li^+/Ala\text{-}C]_{aq}$ show that the bidentate coordination of Li^+ at the O1 and N atoms of Ala-C leads to a significant increase in the degree of hydration, especially at the COOH and NH_2 groups. In $[Li^+/Ala\text{-}C]_{aq}$, all g(R) related to the O2–H7...Ow and N–H...Ow H-bonds are in general

Notes to Table 2
ΔEa^{AW-WW} = activation interaction energy of the water exchange intermediate complex.
[a] The abbreviation for the water exchange mechanism taken from Langford and Gray [65].

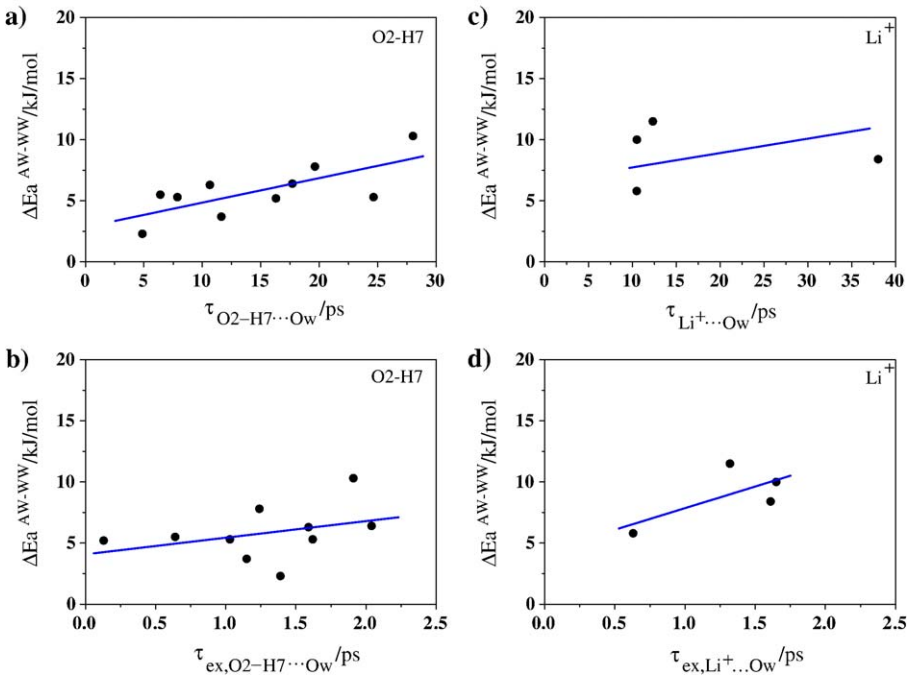

Fig. 10. Selected correlation diagrams obtained from MD simulations of MD-$[Ala]_{aq}$ and MD-$[Li^+/Ala\text{-}C]_{aq}$ at 298 K. (a) ΔE^{AW-WW} and $\tau_{O2-H7...Ow}$. (b) ΔE^{AW-WW} and $\tau_{ex,O2-H7...Ow}$. (c) ΔE^{AW-WW} and $\tau_{Li^+...Ow}$. (d) ΔE^{AW-WW} and $\tau_{ex,Li^+...Ow}$.

more structured compared to those in $[Ala\text{-}C]_{aq}$. The positions of the main peaks of $g(R_{O2...Ow})$, $g(R_{H7...Ow})$ and $g(R_{N...Ow})$ are also shifted to shorter distances; whereas those of $g(R_{H2...Ow})$ and $g(R_{H3...Ow})$ become more equivalent, compare Fig. 6e and g, and f and h, respectively. The integrations of $g(R_{O2...Ow})$ and $g(R_{N...Ow})$ to the first maxima showed that, upon the Li^+ binding, the number of water molecule in close contact with the COOH and NH_2 groups are increased from 1.84 to 2.08 and from 1.7 to 2.0, respectively.

The structure of $g(R_{Li^+...Ow})$ in Fig. 6i indicates that the first and second hydration shells of Li^+/Ala-C are not as well separated as in $[Li^+]_{aq}$ [43,44]. This suggests that Li^+ becomes softer due to the bidentate coordination with Ala, and water molecules in the first hydration shell of Li^+ could be more dynamics. $g(R_{Li^+...Ow})$ shows the first maximum and minimum at 2.01 and 2.96 Å, respectively. They are slightly longer than those in $[Li^+]_{aq}$ [44], 1.96 and 2.70 Å, respectively. The integrations of $g(R_{Li^+...Ow})$ to the first maximum and minimum yielded one (1.02) water molecule in close contact with Li^+ and about three (3.17) water molecules in the first hydration shell of Li^+/Ala-C. The number of water molecules in the first hydration shell is quite reasonable, compared with four (4.02) in the case of $[Li^+]_{aq}$ [44]. The slightly larger first hydration shell with smaller number of water molecule in $[Li^+/Ala\text{-}C]_{aq}$ compared to $[Li^+]_{aq}$ could also be attributed to the steric effects caused by the bidentate coordination at Li^+.

The hydration structures and the total–average potential energy landscapes at the H-bond networks of Ala-C are obviously affected by the Li^+ binding. Comparisons of the PDO maps in Fig. 7l and p and the total–average potential energy landscapes in Fig. 8i to l show that Li^+ can transfer its electrostatic effects to the O2–H7 group, leading to a more associated H-bond network at A, as well as higher average potential energy barriers for the diffusion of water molecule in the transverse direction ($\langle \Delta E_{aq}^{T} \rangle$) in $[Li^+/Ala\text{-}C]_{aq}$ compared to $[Ala\text{-}C]_{aq}$. These lead to longer $\tau_{O2-H7...Ow,max}$ in $[Li^+/Ala\text{-}C]_{aq}$, compared to $[Ala\text{-}C]_{aq}$, 28.0 and 20.4 ps, respectively. The values of $\tau_{O2-H7...Ow,max}$ correspond to the water exchange rate constants (k_{ex}) of 35.7 and 49.1 ns^{-1}, respectively. The binding of Li^+ at the O1 and N groups of Ala-C also strengthens and lengthens the H-bond networks at the NH_2 group; the H-bond networks at D, G and I become more well defined and interconnected, as seen in Fig. 7l and q. This further suggests that the hydration at the CH groups is increased upon the Li^+ binding, with the longest H-bond lifetime $\tau_{N-H3...Ow,max}$ increasing from about 17 ps in $[Ala\text{-}C]_{aq}$ to about 18 ps in $[Li^+/Ala\text{-}C]_{aq}$.

The three water molecules in the first hydration shell of Li^+/Ala-C were found to distribute in four H-bond networks labeled with M to P on the PDO maps in Fig. 7p to t, with quite high contour densities at P and M. The structures of the total–average potential energy landscapes and the cross section plots in Fig. 8m to r show that water molecules in the first hydration shell of Li^+ could be moving in narrow channels interconnecting the four H-bond networks, with $\langle \Delta E_{aq}^{L} \rangle$ of about 10 kJ/mol. The structures of the cross section plots deduced from the transverse profile lines suggested longer water residence time at Li^+ compared to those at the COOH and NH_2 groups, with $\langle \Delta E_{aq}^{T} \rangle$ at P and M of 108–110 kJ/mol, respectively. $\tau_{Li^+...Ow,max}$ derived from MD-$[Li^+/Ala\text{-}C]_{aq}$ is about 38 ps, corresponding to the water exchange rate constant ($\tau_{ex,\ Li^+...Ow}$) of 26.3 ns^{-1}, see Table 1. As mentioned earlier that the water residence times are quite sensitive to the definitions and methods employed in the investigations, rigorous comparison could not be made easily. The average residence time of water molecule in the first

hydration shell of Li^+ has been determined by quasi-elastic neutron scattering (QENS) [71] to be less than 100 ps, whereas the MD results compiled in Ref. [44] are ranging from 25 and 400 ps. Our $\tau_{Li^+...Ow,max}$ seems to be in reasonable agreement with those estimated from *ab initio* MD simulations, ranging from 20 and 50 ps [72].

Due to limited number of complete water exchange events taking place in the first hydration shell of Li^+, the water exchange diagrams obtained from MD-$[Li^+/Ala\text{-}C]_{aq}$ could not be examined as extensive as in $[Ala\text{-}A]_{aq}$, $[Ala\text{-}B]_{aq}$ and $[Ala\text{-}C]_{aq}$. Some representative results are given in Fig. 10 and their analyses in Table 2b. It appeared that, in $[Li^+/Ala\text{-}C]_{aq}$, the I mechanisms were observed more often than the D mechanism, with $\tau_{Li^+...Ow}$ and $\tau_{ex,Li^+...Ow}$ varying from 10.5 to 38.0 ps and from 0.6 to 1.6 ps, respectively. The suggested mechanisms agree well with the MD results in Ref. [43], in which the I_d and D mechanisms were reported to dominate in $[Li^+]_{aq}$.

Further investigations on MD trajectories, shown as examples in Fig. 9h, revealed that water molecule (W151) enters the first hydration shell of the O2–H7 group and moves inside the average potential energy channel for a while, before leaving the channel at some point, and in general, water molecule could enter and leave the first hydration shell at various points in the channel. This implies that the frequency of the water exchange events depends to some extent on this dynamic step. Therefore, this dynamic step should be included in the water exchange pathways of amino acid. Our suggestion seems to comply with the observations made in Ref. [44] that a complete understanding of the water exchange mechanisms requires information on both hydration structures and dynamics, which are closely related to the interactions and momentum transfer between water molecules in the first and second hydration shells. The influence of water molecules in the second hydration shell was also illustrated in our previous work on $[NH_4^+]_{aq}$ [73] and $[H_3O^+]_{aq}$ [74]. Especially in the case of $[H_3O^+]_{aq}$ [74], it was shown that water molecules in the second hydration shell could help promote the proton transfer from H_3O^+ to H_2O, through the formation of the Zundel complex ($H_5O_2^+$).

The MD trajectory in Fig. 9h also shows that water molecule (W15) moves back and forth inside the average potential energy channel interconnecting the H-bond networks at M, N, O and P, as in the case of the O2–H7 group, with the time interval between successive water exchange events of about 10 ps, see Fig. 9e to g and Table 2b. Since the values of $\tau_{ex,Li^+...Ow}$, shown in Table 2b, are considerably smaller than $\tau_{Li^+...Ow}$ and vary only in a narrow range, between 0.6 and 1.6 ps, the diffusion of water molecule in the average potential energy channel could be a rate-determining step and should be included, as an additional dynamic step, in the water exchange process. The correlation diagrams in Fig. 10c and d reveal the trends of $\tau_{Li^+...Ow}$ and ΔEa^{AW-WW}, and $\tau_{ex,Li^+...Ow}$ and ΔEa^{AW-WW} similar to $[Ala]_{aq}$.

It should be noted that the water exchange mechanisms proposed by Langford and Gray [65], as well as the others [69], emphasize the stereochemistry (*cis* or *trans*) of each exchange event, by trying to correlate the five-water exchange mechanisms with the degree of contraction or expansion of the first hydration shell during the water exchange process. In addition, the present MD results focus attention on the dynamics of water molecule in the first hydration shell of solute and propose to include this dynamic step in the water exchange process.

4. Conclusion

The effects of metal ion and solute conformation change on the structures, energetic and dynamics of water molecule in the first hydration shell of amino acid were examined, using alanine (Ala) and Li^+/Ala as model molecules. The present theoretical studies began with the constructions of the test-particle model (T-model) potentials for four structures of Ala, regarded as Ala-A, Ala-B, Ala-C and Li^+/Ala-C; Ala-B and Ala-C were generated from Ala-A by rotations of the N–C^α bond 30° and 180°, respectively. The T-model potentials were applied in the calculations of the optimal geometries of the Ala–H_2O 1:*n* complexes in the gas phase, with $n=1$ to 4. Some of the T-model results were examined using *ab initio* calculations at MP2 level of theory. The T-model potentials and MP2 calculations yielded comparable results. They suggested that, for all the Ala–H_2O complexes considered, water molecules prefer to form cyclic H-bonds at the COOH group, with similar H-bond structures and interaction energies. In the gas phase, the variation of the angle ϕ from 0° to 30° to 180° does not bring about significant change on the hydration at the COOH group, whereas some effects were observed at the NH_2 groups, especially when the angle $\phi=180°$. A three-center or bifurcated H-bond, in which only one Ow–Hw group of water approaches simultaneously at the N and O1 atoms, was detected in the Ala-C–H_2O 1:1 complexes.

For Li^+/Ala-C, water molecule prefers to bind primarily at Li^+, and subsequently at the COOH and NH_2 groups. It appears that, in the gas phase, not more than two water molecules bind directly at Li^+, compared to four in the case of Li^+/H_2O. The number of water molecules is in good agreement with *ab initio* calculations on the Li^+/Val 1:2 and 1:3 complexes. The bidentate coordination of Li^+ at the N and O1 atoms of Ala-C brings about significant changes at both COOH and NH_2 groups, for which the structure of the O2–H7…Ow H-bond is most affected, with an increase in the H-bond interaction energy. The linear O–H…Ow H-bond becomes favorable upon the Li^+ binding. Based on the results discussed above, one can conclude that the T-model potentials predicted reasonable gas-phase equilibrium structures and interaction energies for all the Ala–H_2O and Li^+/Ala-C–H_2O 1:*n* complexes and can be applied in MD simulations with confidence.

MD simulations were performed on $[Ala\text{-}A]_{aq}$, $[Ala\text{-}B]_{aq}$, $[Ala\text{-}C]_{aq}$ and $[Li^+/Ala]_{aq}$ at 298 K, using the T-model potentials. The MD results showed that the rotation of the N–C^α bond from the angle $\phi=0°$ to 30° to 180° brings about different effects to the H-bond networks, compared to the gas phase. MD-$[Ala\text{-}A]_{aq}$ and MD-$[Ala\text{-}B]_{aq}$ revealed that the variation of the angle ϕ from 0° to 30° strengthens the H-bond networks at the O2–H7 and C1–H1 groups and weakens the ones at the lone-pair electrons of O1 and the NH_2 groups. The stabilities of the H-bond networks at the COOH and NH_2 groups are further increased and decreased, respectively, when the angle ϕ is

changed from 30° to 180°, with additional H-bond networks created upon the rotation. The dynamics of water molecules in the first hydration shells of solutes were illustrated again to be attributable from the structures of the total–average potential energy landscapes. Although not so straightforward, it was shown that the values of the longest H-bond lifetimes could reflect the structures of the total–average potential energy landscapes and vice versa. The MD analyses employed in the present work could be applied in the investigation of the diffusion of water molecules at the protein surfaces, known in general as the lateral and transversal diffusions.

The structural and energetic results obtained from MD simulations showed that the bidentate coordination of Li^+ at N and O1 brings about considerable stabilization effects to all H-bond networks in $[Li^+/Ala]_{aq}$. It appeared that the H-bond networks at the O2–H7 and the NH_2 groups become more associated, with increases in the average potential energy barriers to the diffusion of water molecules between the H-bond network and the outside. Three water molecules are in the first hydration shell of Li^+. They seem to distribute in four associated H-bond networks, which are interconnected and form an average potential energy channel for the diffusion of water molecules. The analyses of the water exchange diagrams and MD trajectories in $[Li^+/Ala]_{aq}$ suggested to include an elementary dynamic step to the water exchange process, in which water molecules move in a channel in the first hydration shell before leaving at some points in the channel.

It should be noted that the MD results reported in the present work were based on pair-wise additive intermolecular potentials, in which the many-body contributions were not taken into account. Although the electrostatic effects introduced by Li^+ are relatively strong, the treatment of Li^+/Ala as a supermolecule could partly compromise these effects and our approximated rigid model could represent one of the most probable states in $[Li^+/Ala\text{-}C]_{aq}$. The inclusion of the cooperative effects in our model calculations is expected to result in slightly more associated H-bond networks, as well as longer water residence times, and should not bring about significant change in the reported results. The theoretical results presented here also iterate the necessity to include explicit solvent molecules in the model calculations. Since the microscopic nature of water molecules in aqueous solutions cannot be directly accessible from experiments, the authors hope that the present work could provide additional important information on the structures, energetic and dynamics of water molecules in the hydration shells of amino acids.

Acknowledgement

All calculations were performed at School of Chemistry and School of Mathematics, Suranaree University of Technology. The authors would like to acknowledge the financial support from the Thailand Research Fund (TRF) through the Royal Golden Jubilee (RGJ) PhD program (Grant No. PHD/0005/2542) to Natthiya Deeying and Prof. Dr. Kritsana Sagarik. Valuable suggestions and comments from Prof. Dr. Osamu Kikuchi, University of Tsukuba, Japan, are greatly acknowledged.

References

[1] S.A. Lippard, J.M. Berg, Principles of Bioinorganic Chemistry, University Science Books, Mill Valley, CA, 1994.
[2] B.A. Cerda, C. Wesdemiotis, Li^+, Na^+, and K^+ binding to the DNA and RNA nucleobases. Bond energies and attachment sites from the dissociation of metal ion-bound heterodimers, J. Am. Chem. Soc. 118 (1996) 11884–11892.
[3] M.N. Hughes, The Inorganic Chemistry of Biological Process, 2nd ed. John Wiley and Sons, Chichester, 1981.
[4] W.G. Zhong, J.P. Gallivan, Y.N. Zhang, L.T. Li, H.A. Lester, D.A. Dougherty, From *ab initio* quantum mechanics to molecular neurobiology: a cation-π binding site in the nicotinic receptor, Proc. Natl. Acad. Sci. U. S. A. 95 (1998) 12088–12093.
[5] J.A. Leary, Z. Zhou, S.A. Ogden, T.D. Williams, Investigations of gas-phase lithium-peptide adducts: tandem mass spectrometry and semiempirical studies, J. Am. Soc. Mass Spectrom. 1 (1990) 473–480.
[6] H.J. Dyson, P.E. Wright, Unfolded proteins and protein folding studied by NMR, Chem. Rev. 104 (2004) 3607–3622.
[7] R.B. Gregory (Ed.), Protein–Solvent Interactions, Marcel Dekker, New York, 1994.
[8] R.M. Moision, P.B. Armentrout, Experimental and theoretical dissection of sodium cation/glycine interactions, J. Phys. Chem., A 106 (2002) 10350–10362.
[9] E.F. Strittmatter, A.S. Lemoff, E.R. Williams, Structure of cationized glycine, gly·M^{2+} (M = Be, Mg, Ca, Sr, Ba), in the gas phase: intrinsic effect of cation size on zwitterion stability, J. Phys. Chem., A 104 (2000) 9793–9796.
[10] R.A. Jockusch, A.S. Lemoff, E.R. Williams, Effect of metal ion and water coordination on the structure of a gas-phase amino acid, J. Am. Chem. Soc. 123 (2001) 12255–12265.
[11] R.A. Jockusch, W.D. Price, E.R. Williams, Structure of cationized arginine (Arg·M^+, M = H, Li, Na, K, Rb, and Cs) in the gas phase: further evidence for zwitterionic arginine, J. Phys. Chem., A 103 (1999) 9266–9274.
[12] F. Jensen, Structure and stability of complexes of glycine and glycine methyl analogs with H^+, Li^+, and Na^+, J. Am. Chem. Soc. 114 (1992) 9533–9537.
[13] T. Marino, N. Russo, M. Toscano, Gas-phase metal ion (Li^+, Na^+, Cu^+) affinities of glycine and alanine, J. Inorg. Biochem. 79 (2000) 179–185.
[14] T. Marino, N. Russo, M. Toscano, Potential energy surfaces for the gas-phase interaction between α-alanine and alkali metal ions (Li^+, Na^+, K^+). A density functional study, Inorg. Chem. 40 (2001) 6439–6443.
[15] T. Wyttenbach, M. Witt, M.T. Bowers, On the question of salt bridges of cationized amino acids in the gas phase: glycine and arginine, Int. J. Mass Spectrom. 182–183 (1999) 243–252.
[16] F.M. Siu, N.L. Ma, C.W. Tsang, Cation-π interactions in sodiated phenylalanine complexes: is phenylalanine in the charge-solvated or zwitterionic form? J. Am. Chem. Soc. 123 (2001) 3397–3398.
[17] B.M. Rode, K.P. Sagarik, The influence of small monovalent cations on neighbouring N...H–O hydrogen bonds, Chem. Phys. Lett. 88 (1982) 337–341.
[18] K.P. Sagarik, B.M. Rode, The influence of small monovalent cations on neighbouring hydrogen bonds of aquo-protein complexes, Z. Naturforsch. 36a (1981) 1357–1360.
[19] K.P. Sagarik, B.M. Rode, The influence of small monovalent cations on the hydrogen bonds of base pair of DNA, Ing. Chim. Acta 78 (1983) 81–86.
[20] K.P. Sagarik, B.M. Rode, Quantum chemical investigations on group IA and IIA metal ion-DNA base complexes, Ing. Chim. Acta 76 (1983) L209–L212.
[21] X. Du, Y. Liang, Roles of metal complex and hydrogen bond in molecular structures and phase behaviors of metal *N*-octadecanoyl-L-alaninate Langmuir-Blodgett films, J. Phys. Chem., B 104 (2000) 10047–10052.
[22] J.L. Finney, A.K. Soper, Solvent structure and perturbations in solutions of chemical and biological importance, Chem. Soc. Rev. 23 (1994) 1–10.
[23] K.A. Dill, Dominant forces in protein folding, Biochemistry 29 (1990) 7133–7155.
[24] M.U. Palma, M.B. Palma-Vittorelli, F. Parak (Eds.), Water–Biomolecule Interactions; Conference Proceedings, vol. 43, SIF, Bologna, 1993.
[25] W. Saenger, Structure and dynamics of water surrounding biomolecules, Annu. Rev. Biophys. Biophys. Chem. 16 (1987) 93–114.

[26] M. Levitt, B.H. Park, Water: now you see it, now you don't, Structure 1 (1993) 223–226.
[27] S. Saigal, J. Pranata, Monte Carlo simulations of guanidinium acetate and methylammonium acetate ion pairs in water, Bioorg. Chem. 25 (1997) 11–21.
[28] X. Rozanska, C. Chipot, Modeling ion–ion interaction in proteins: a molecular dynamics free energy calculation of the guanidinium–acetate association, J. Chem. Phys. 112 (2000) 9691–9694.
[29] W.F. van Gunsteren, H.J.C. Berendsen, J. Hermans, W.G.J. Hol, J.P.M. Postma, Computer simulation of the dynamics of hydrated protein crystals and its comparison with X-ray data, Proc. Natl. Acad. Sci. U. S. A. 80 (1983) 4315–4319.
[30] G. Otting, K. Wuethrich, Studies of protein hydration in aqueous solution by direct NMR observation of individual protein-bound water molecules, J. Am. Chem. Soc. 111 (1989) 1871–1875.
[31] G. Otting, E. Liepinsh, K. Wuethrich, Polypeptide hydration in mixed solvents at low temperatures, J. Am. Chem. Soc. 114 (1992) 7093–7095.
[32] K. Wuethrich, Hydration of biological macromolecules in solution: surface structure and molecular recognition, in: K. Wuethrich (Ed.), NMR in Structural Biology, World Scientific Series in 20th Century Chemistry, vol. 5, World Scientific, Singapore, 1995, p. 647.
[33] M. Odelius, A. Laaksonen, Combined MD simulation-NMR relaxation studies of molecular motion and intermolecular interactions, in: P.B. Balbuena, J.M. Seminario (Eds.), Molecular Dynamics from Classical to Quantum Methods, Theoretical and Computational Chemistry, vol. 7, Elsevier, Amsterdam, 1999, p. 281.
[34] R.M. Brunne, E. Liepinsh, G. Otting, K. Wüthrich, W.F. van Gunsteren, Hydration of proteins: a comparison of experimental residence times of water molecules solvating the bovine pancreatic trypsin inhibitor with theoretical model calculations, J. Mol. Biol. 231 (1993) 1040–1048.
[35] E.W. Knapp, I. Muegge, Heterogeneous diffusion of water at protein surfaces: application to BPTI, J. Phys. Chem. 97 (1993) 11339–11343.
[36] I. Muegge, E.W. Knapp, Residence times and lateral diffusion of water at protein surfaces: application to BPTI, J. Phys. Chem. 99 (1995) 1371–1374.
[37] M. Orozco, F.J. Luque, Theoretical methods for the representation of solvent in biomolecular systems, Chem. Rev. 100 (2000) 4187–4225.
[38] K. Sagarik, S. Dokmaisrijan, A theoretical study on hydration of alanine zwitterions, J. Mol. Struct., Theochem. 718 (2005) 31–47.
[39] K. Sagarik, S. Chaiyapongs, Structures and stability of salt-bridge in aqueous solution, Biophys. Chem. 117 (2005) 18–39.
[40] K. Sagarik, B.M. Rode, Intermolecular potential for benzoic acid–water based on the test-particle model and statistical mechanical simulations of benzoic acid in aqueous solutions, Chem. Phys. 260 (2000) 159–182.
[41] K. Sagarik, S. Chaiwongwattana, P. Sisot, A theoretical study on clusters of benzoic acid–water in benzene solutions, Chem. Phys. 306 (2004) 1–12.
[42] E. Clementi, Computational Aspects for Large Chemical Systems, Lecture Notes in Chemistry, vol. 19, Springer-Verlag, Berlin, 1980.
[43] K. Hermansson, M. Wojcik, Water exchange around Li^+ and Na^+ in LiCl(aq) and NaCl(aq) from MD simulations, J. Phys. Chem., B 102 (1998) 6089–6097.
[44] D. Spångberg, R. Rey, J.T. Hynes, K. Hermansson, Rate and mechanisms for water exchange around Li^+(aq) from MD simulations, J. Phys. Chem., B 107 (2003) 4470–4477.
[45] H.A. Levy, R.B. Corey, The crystal structure of DL-alanine, J. Am. Chem. Soc. 63 (1941) 2095–2108.
[46] J. Donohue, The crystal structure of DL-alanine: II. Revision of parameters by three-dimensional Fourier analysis[1], J. Am. Chem. Soc. 72 (1950) 949–953.
[47] S.G. Stepanian, I.D. Reva, E.D. Radchenko, L. Adamowicz, Conformational behavior of α-alanine. Matrix-isolation infrared and theoretical DFT and ab initio study, J. Phys. Chem., A 102 (1998) 4623–4629.
[48] I.D. Reva, A.M. Plokhotnichenko, S.G. Stepanian, A.Yu. Ivanov, E.D. Radchenko, G.G. Sheina, Y.P. Blagoi, The rotamerization of conformers of glycine isolated in inert gas matrices. An infrared spectroscopic study, Chem. Phys. Lett. 232 (1995) 141–148.
[49] R.D. Suenram, F.J. Lovas, Millimeter wave spectrum of glycine. A new conformer, J. Am. Chem. Soc. 102 (1980) 7180–7184.
[50] A.G. Csazar, On the structures of free glycine and α-alanine, J. Mol. Struct. 346 (1995) 141–152.
[51] D.S. Ahn, S.W. Park, I.S. Jeon, M.K. Lee, N.H. Kim, Y.H. Han, S. Lee, Effects of microsolvation on the structures and reactions of neutral and zwitterion alanine: computational study, J. Phys. Chem., B 107 (2003) 14109–14118.
[52] C.H. Hu, M. Shen, H.F. Schaefer III, Glycine conformational analysis, J. Am. Chem. Soc. 115 (1993) 2923–2929.
[53] J.H. Jensen, M.S. Gordon, Conformational potential energy surface of glycine: a theoretical study, J. Am. Chem. Soc. 113 (1991) 7917–7924.
[54] F.R. Tortonda, J.L. Pascual-Ahuir, E. Silla, I. Tuñón, A theoretical study of solvent effects on the conformational equilibria of neutral glycine in aqueous solution, J. Mol. Struct., Theochem. 623 (2003) 203–210.
[55] E.N. Baker, R.E. Hubbard, Hydrogen bonding in globular proteins, Prog. Biophys. Mol. Biol. 44 (1984) 97–179.
[56] E. Clementi, F. Cavallone, R. Scordamaglia, Analytical potentials from "*ab initio*" computations for the interaction between biomolecules: 1. Water with amino acids, J. Am. Chem. Soc. 99 (1977) 5531–5545.
[57] K. Sagarik, Theoretical studies on hydrogen bonding in hydroxylamine clusters and liquid, J. Mol. Struct., Theochem. 465 (1999) 141–155.
[58] L.F. Pacios, P.C. Gómez, Atomic charges in conformers of gaseous glycine, J. Mol. Struct., Theochem. 544 (2001) 237–251.
[59] C.M. Breneman, K.B. Wiberg, Determining atom-centered monopoles from molecular electrostatic potentials. The need for high sampling density in formamide conformational analysis, J. Comput. Chem. 11 (1990) 361–373.
[60] M.J. Frisch, G.W. Trucks, H.B. Schlegel, G.E. Scuseria, M.A. Robb, J.R. Cheeseman, V.G. Zakrzewski, J.A. Montgomery, R.E. Stratmann, J.C. Burant, S. Dapprich, J.M. Millam, A.D. Daniels, K.N. Kudin, M.C. Strain, O. Farkas, J. Tomasi, V. Barone, M. Cossi, R. Cammi, B. Mennucci, C. Pomelli, C. Adamo, S. Clifford, J. Ochterski, G.A. Petersson, P.Y. Ayala, Q. Cui, K. Morokuma, D.K. Malick, A.D. Rabuck, K. Raghavachari, J.B. Foresman, J. Cioslowski, J.V. Ortiz, B.B. Stefanov, G. Lui, A. Liashenko, P. Piskorz, I. Komaromi, R. Gomperts, R.L. Martin, D.J. Fox, T. Keith, M.A. Al-Laham, C.Y. Peng, A. Nanayakkara, C. Gonzalez, M. Challacombe, P.M.W. Gill, B.G. Johnson, W. Chen, M.W. Wong, J.L. Andres, M. Head-Gordon, E.S. Replogle, J.A. Pople, Gaussian 98, Gaussian, Inc., Pittsburgh, 1998.
[61] A.G. Csaszar, Conformers of gaseous glycine, J. Am. Chem. Soc. 114 (1992) 9568–9575.
[62] H.B. Schlegel, Optimization of equilibrium geometries and transition structures, J. Comput. Chem. 3 (1982) 214–218.
[63] M.P. Allen, D.J. Tildesley, Computer Simulation of Liquids, Oxford University Press, New York, 1989.
[64] SURFER for Window, version 6.04, Golden Software, Inc., U.S.A., 1997.
[65] C.H. Langford, H.B. Gray, Ligand Substitution Processes, W.A. Benjamin, New York, 1996.
[66] O.Y. Kwon, S.Y. Kim, K.T. No, Determination of the proton transfer energies of glycine and alanine and the influence of water molecules, Bull. Korean Chem. Soc. 16 (1995) 410–416.
[67] J. Donohue, in: A. Rich, N. Davidson (Eds.), Structure Chemistry and Molecular Biology, W.H. Freeman, San Francisco, 1968, p. 443.
[68] G.A. Jeffrey, W. Saenger, Hydrogen Bonding in Biological Structures, Springer-Verlag, Berlin, 1991.
[69] R. Puchta, M. Galle, N. van Eikema Hommes, E. Pasgreta, R. van Eldik, Evidence for associative ligand exchange processes on solvated lithium cations, Inorg. Chem. 43 (2004) 8227–8229.
[70] J. Middlehurst, in: R. Harrison (Ed.), Practical Filter Design, Prentice Hall, Brunswick, 1993.
[71] P.S. Salmon, W.S. Howells, R. Mills, The dynamics of water molecules in ionic solution: II. Quasi-elastic neutron scattering and tracer diffusion studies of the proton and ion dynamics in concentrated Ni^{2+}, Cu^{2+} and Nd^{3+} aqueous solutions, J. Phys. C. Solid State Phys. 20 (1987) 5727–5747.
[72] A.P. Lyubartsev, K. Laasonen, A. Laaksonen, Hydration of Li^+ ion. An *ab-initio* molecular dynamics simulation, J. Chem. Phys. 114 (2001) 3120–3126.
[73] P. Intharathep, A. Tongraar, K. Sagarik, Structure and dynamics of hydrated NH_4^+: an ab initio QM/MM molecular dynamics simulation, J. Comput. Chem. 26 (2005) 1329–1338.
[74] P. Intharathep, A. Tongraar, K. Sagarik, in press. *Ab initio* QM/MM dynamics of H_3O^+ in water. J. Compt. Chem.